A&A 399, 147–167 (2003)
DOI: 10.1051/0004-6361:20021717

Astronomy & Astrophysics

Star formation in the Vela molecular clouds⋆,⋆⋆

V. Young stellar objects and star clusters towards the C-cloud

F. Massi[1], D. Lorenzetti[2], and T. Giannini[2]

[1] Osservatorio Astrofisico di Arcetri, INAF, Largo E. Fermi 5, 50125 Firenze, Italy
[2] Osservatorio Astronomico di Roma, INAF, Via Frascati 33, 00040 Monte Porzio Catone, Roma, Italy
e-mail: dloren@coma.mporzio.astro.it, teresa@coma.mporzio.astro.it

Received 4 July 2002 / Accepted 14 November 2002

Abstract. We present the latest results from a sensitive ($K \sim 18$ mag) near-infrared (JHK) imaging survey of IRAS selected young stellar objects associated with the Vela molecular ridge. These enlarge the sample of 12 fields, previously studied, adding 10 sites of recent star formation. The spectral energy distributions derived from near-infrared and 1.3-mm photometry allowed to identify at least 5 Class I sources. Their bolometric luminosities indicate that they are protostellar objects of intermediate mass (∼2–10 $M_\odot$). Herbig Ae/Be stars and compact UCHII regions could account for the far infrared emission towards some of the remaining fields. The most luminous IRAS sources have also been found associated with young embedded star clusters. The physical properties of the clusters have been determined and used to improve on the statistical relationships already suggested by our previous work. They have sizes of ≳0.1 pc and volume densities of 10^3–10^4 stars pc^{-3}. Where identified, the Class I sources tend to lie near the centre of the clusters and it is confirmed that the most massive ones are associated with the richest clusters. The less luminous Class I sources (∼10^2 $L_\odot$) are found either isolated or within small groups of young stellar objects. It is proposed to use the relationship between the bolometric luminosity of the IRAS sources and the total number of cluster members as a test of the initial mass function at the highest masses.

Key words. stars: formation – stars: pre-main sequence – infrared: stars – ISM: individual objects: Vela molecular ridge

1. Introduction

The far-infrared (FIR) maps of the sky provided by the IRAS satellite have long been a cornerstone in driving a number of studies on star formation processes. Along the same lines, Liseau et al. (1992) and Lorenzetti et al. (1993), hereafter Paper I and Paper II respectively, used the IRAS Point Source Catalogue (PSC) for retrieving all listed sources with colours typical of young stellar objects on the sky area of the Vela Molecular Ridge (VMR) as designated by Murphy & May (1991). The VMR is a giant molecular cloud complex located *in* the galactic plane ($b \approx \pm 3°$) outside the solar circle ($l \approx 260°$–$275°$). Murphy & May (1991) delineated its structure by low resolution (∼30′) mm-observations in the CO(1 – 0) transition. These authors further subdivided the emission area into 4 main regions (named A, B, C and D) based on the location of the intensity peaks. The issue of distance is discussed in Paper I, where a value of 700 ± 200 pc is derived for clouds A, C and D. Details on the VMR and its star formation history can be found in the quoted literature.

Complementing the selected PSC entries with near-infrared (NIR) single-channel photometry and mm observations, a Spectral Energy Distribution (SED) is determined for each object and a catalogue of Class I sources (Lada & Wilking 1984) associated with the VMR is eventually provided in Papers I and II. More precisely, given the bolometric luminosities implied by the FIR fluxes (10^2–10^4 $L_\odot$), these objects are actually the analogues of Class I sources in the regime of intermediate mass stars (2–10 $M_\odot$). An analysis of the large scale star formation activity hosted by the VMR is attempted in Papers I and II, as well. Due to the intrinsic low resolution of IRAS data and NIR single channel photometry, the issue of the environmental effects on the derived SEDs could not be addressed in the two works. Hence, Massi et al. (1999) and Massi et al. (2000), hereafter Paper III and Paper IV, studied NIR images (JHK) of a subsample of 12 sources (all those listed in the final

Send offprint requests to: F. Massi,
e-mail: fmassi@arcetri.astro.it

⋆ Based on observations collected at the European Southern Observatory, Chile.

⋆⋆ The complete version of Table 5 is only available in electronic form at the CDS via anonymous ftp to cdsarc.u-strasbg.fr (130.79.128.5) or via
http://cdsweb.u-strasbg.fr/cgi-bin/qcat?J/A+A/399/147

catalogue of Papers I-II and believed to belong to cloud D) in order to find out the counterparts of the FIR emission. These images also unveiled the presence of a number of young embedded star clusters among the most luminous IRAS sources. These are discussed in Paper IV. The preliminary results of larger field and much deeper NIR imaging towards a few of the IRAS sources studied in Papers III–IV (Testi et al. 2001) confirm the findings of Paper IV on the embedded young clusters. Another feature of the sites hosting the IRAS sources is sketched by Lorenzetti et al. (2002) who searched for protostellar jets towards the 12 sources of Papers III–IV (and 3 more ones, also associated with the VMR) using NIR imaging in narrow bands centred at the 2.12 μm transition of H_2 and at the 1.7 μm transition of [FeII]. The case of a well developed jet discovered towards IRS 17 (also known as IRAS 08448–4343) is examined in detail with the aid of NIR spectroscopy.

A few important recent works on observations at mm wavelengths are worth to be mentioned. Wouterloot & Brand (1999) observed ^{12}CO(1 − 0), ^{13}CO(1 − 0), C^{18}O(1 − 0) and CS(2 − 1) towards nine sources in the Vela region, presenting maps of molecular clumps and unveiling the presence of a few molecular outflows. Four of the sources are listed in the catalogue of Papers I–II and are among those studied in Papers III–IV. But the most important advancement in the mm range is represented by the results of the large scale observations with NANTEN: Yamaguchi et al. (1999) present new large-scale higher-resolution (∼3′) maps of integrated emission in the ^{12}CO(1 − 0), ^{13}CO(1 − 0) and C^{18}O(1 − 0) transitions. These observations allow to better delineate the morphology and structure of the VMR (see Fig. 1 for the ^{13}CO map) and suggest that cloud C is the less evolved of the complex. The authors also analyse the star formation history in the region, comparing their mm data with the locations of IRAS sources and optical tracers of early evolutionary phases. Moriguchi et al. (2001) discuss the more general distribution of ^{12}CO(1 − 0) towards the Vela Supernova Remnant (SNR) also from NANTEN observations. As for the VMR, they address the possibility of interaction with the SNR, an issue also considered in Paper I where it is shown that the current generation of Class I sources cannot have been induced by compression from the SNR.

In the present paper we attempt to enlarge the study started in Papers III–IV by analysing new *JHK* images towards 10 more IRAS sources, including all those listed in the catalogue of Papers I and II as associated to cloud C. The aim is to search for the counterparts of the FIR emission, to find out new embedded young star clusters and to derive their properties as in Paper IV. All catalogue entries quoted to belong to either cloud C or D have now been looked at in the NIR with high resolution imaging. Observations and data reduction are described in Sect. 2, the results are reported in Sect. 3 and discussed in Sect. 4 and the main conclusions are listed in Sect. 5.

2. Observations and data reduction

2.1. Source selection

Analogously to Paper III, from the list given in Papers I and II (based on the IRAS Point Source Catalogue) we selected the sources meeting the following conditions:

1. having passed through all steps described in Papers I and II and being eventually identified as *Class I protostellar candidates*;
2. belonging to the VMR-C cloud (as designated by Murphy & May 1991).

To these, we added 3 more IRAS sources belonging to the D and C clouds either representing Class I sources which had been previously rejected (IRS 70) or being remarkable for their association with HII regions and young star clusters (IRS 16 and IRS 34). Thus, in both Papers III/IV and the present work we examine a flux-limited sample of 22 IRAS sources with red colours [1 Jy < $F(12\,\mu\text{m}) < F(25\,\mu\text{m}) < F(60\,\mu\text{m})$; in the following, $F(i\,\mu\text{m})$ is abbreviated to F_i] and associated to molecular gas whose velocity is in the typical range of clouds C and D ($0 \lesssim v_{\rm LSR} \lesssim 14$ km s^{-1}).

The 10 IRAS sources are listed in Table 1, along with their equatorial coordinates and the gas velocities obtained from pointed observations in CO and/or CS transitions (see Papers I and II). The last column (# IRS) refers to the internal classification adopted in Papers I and II. In Fig. 1 the positions of all IRAS sources (including those discussed in Paper III) are overlaid on the map of ^{13}CO(1 − 0) integrated intensity taken from Yamaguchi et al. (1999; their Fig. 1b).

2.2. Near-IR imaging: Data reduction, photometry and astrometry

The NIR images were obtained in February 1993 (IRS 16, IRS 22, IRS 26, IRS 70) and in February 1994 (IRS 31, IRS 32, IRS 33, IRS 34, IRS 73, IRS 74) with IRAC2 (Moorwood et al. 1992) on the ESO/MPI 2.2-m telescope at La Silla (Chile) through standard J (1.25 μm), H (1.65 μm) and K (2.20 μm) filters. During the 1993 run, a plate scale of 0.49 arcsec/pixel was used (resulting in a field of view of about 2×2 arcmin^2), whereas, during the 1994 run, a plate scale of 0.27 arcsec/pixel was selected in order to better sample the PSF (resulting in a smaller field of view, roughly 1×1 arcmin^2). For each field, we took a set of 3 images per filter offsetting each one by 30″ (10″ in the 1994 run) along declination. Total on-source integration times are in the range 120–270 s (J), 180–270 s (H) and 270–540 s (K), yielding limiting magnitudes $J \sim 19.5$, $H \sim 18.5$ and $K \sim 18.0$. Due to the presence of extremely bright NIR sources, for IRS 34 a total on-source integration time of 180 s was used in all bands, yielding limiting magnitudes $J \sim H \sim 17.5$ and $K \sim 16.5$. Data were reduced as explained in Paper III, performing the $B - C$, $B - A$ and $C - A$ subtraction between all three images A, B and C per field and filter band and combining them. In the case of IRS 34, however, we also needed to remove the NIR sources from the frames to subtract, each time. This because the brightest objects caused large dips in the sky-subtracted frames which could not be removed by simply thresholding when combining together the 3 images, affecting, in turn, the quality of the photometry.

Our photometric techniques are also described in Paper III, but here we used an aperture of ∼1 *FWHM* (the full width

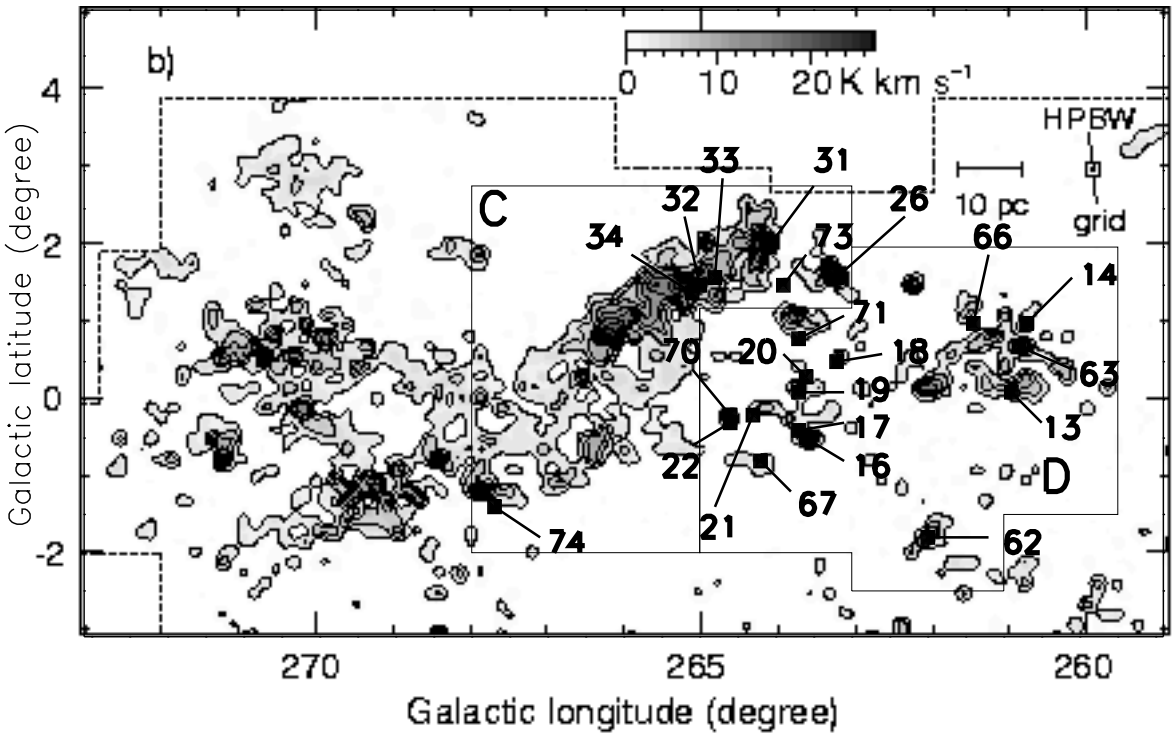

Fig. 1. Spatial distribution of the IRAS Class I sources belonging to cloud C and cloud D (also included those discussed in Paper III), superimposed on the ^{13}CO(1 − 0) integrated intensity map taken from Fig. 1b of Yamaguchi et al. (1999). All sources are labelled according to the nomenclature of Papers I-II. The boundaries of C and D are drawn.

Table 1. Selected IRAS sources.

IRAS name	α(2000.0)			δ(2000.0)			CO: $v_{\rm LSR}$	CS: $v_{\rm LSR}$	$F_{1.3\rm mm}$	# IRS
	h	m	s	°	′	″	(km s^{-1})	(km s^{-1})	(mJy)	
08438-4340	08	45	35.8	−43	51	02	6.0	5.8[a]	-	16
08485-4419	08	50	20.7	−44	30	41	1.20/5.51	2.6[a]	873 ± 50	22
08513-4201	08	53	08.8	−42	13	03	5.4	4.9[a]	510 ± 12	26
08563-4225	08	58	12.5	−42	37	34	8.5	7.5	483 ± 17	31
08575-4330	08	59	21.1	−43	42	06	-	7.0	49 ± 21	32
08576-4314	08	59	25.8	−43	26	07	-	8.6	61 ± 18	33
08576-4334	08	59	25.2	−43	45	45	6.7	7.5	-	34
08485-4414	08	50	15.8	−44	25	57	-	-	-	70
08534-4231	08	55	16.4	−42	43	10	8.3	-	33 ± 11	73
08549-4722	08	56	39.8	−47	34	19	1.6/53.2	-	121 ± 11	74

[a] Bronfman et al. 1996.

at half maximum of the point spread function), an inner annulus of ∼2 *FWHM* and the *median* as a sky estimator. The seeing ranged between 0.8″−1″ during all 1993 and 1994 nights. Furthermore, we carefully selected isolated and bright stars in each field and used the task *mkapfile* in IRAF in order to determine an aperture correction. This resulted in better calibrated colours with respect to Paper III and, possibly, smaller photometric errors. We estimate that errors in aperture corrections and calibration, and residual flat inaccuracies, are as a whole at a $\lesssim 0.1$ mag level. Hence, we expect that the largest photometric errors are caused by source crowdedness and diffuse (variable) emission from extended nebulosities. In order to estimate the latter contribution, we performed experiments with artificial stars of different magnitudes added to different locations of a K image. In uncrowded areas, the difference between recovered magnitudes and true magnitudes increases from 0.014 ± 0.0005 for $K = 12$ mag stars to 0.258 ± 0.194 for $K = 17$ mag stars. In the most extreme conditions (very crowded areas within the wings of extremely bright stars), the difference increases from 0.11 ± 0.09 for $K = 12$ mag stars to 1.6 ± 0.66 for $K = 16$ mag stars; in this case, most of the artificial stars with $K > 16$ mag could not be retrieved, either. As noted in Paper III, we then assumed quite a conservative completeness limit ($K = 15.5$ mag) which accounts both for these local variations within the same image and for variations from image to image. We found that the measured brightness in

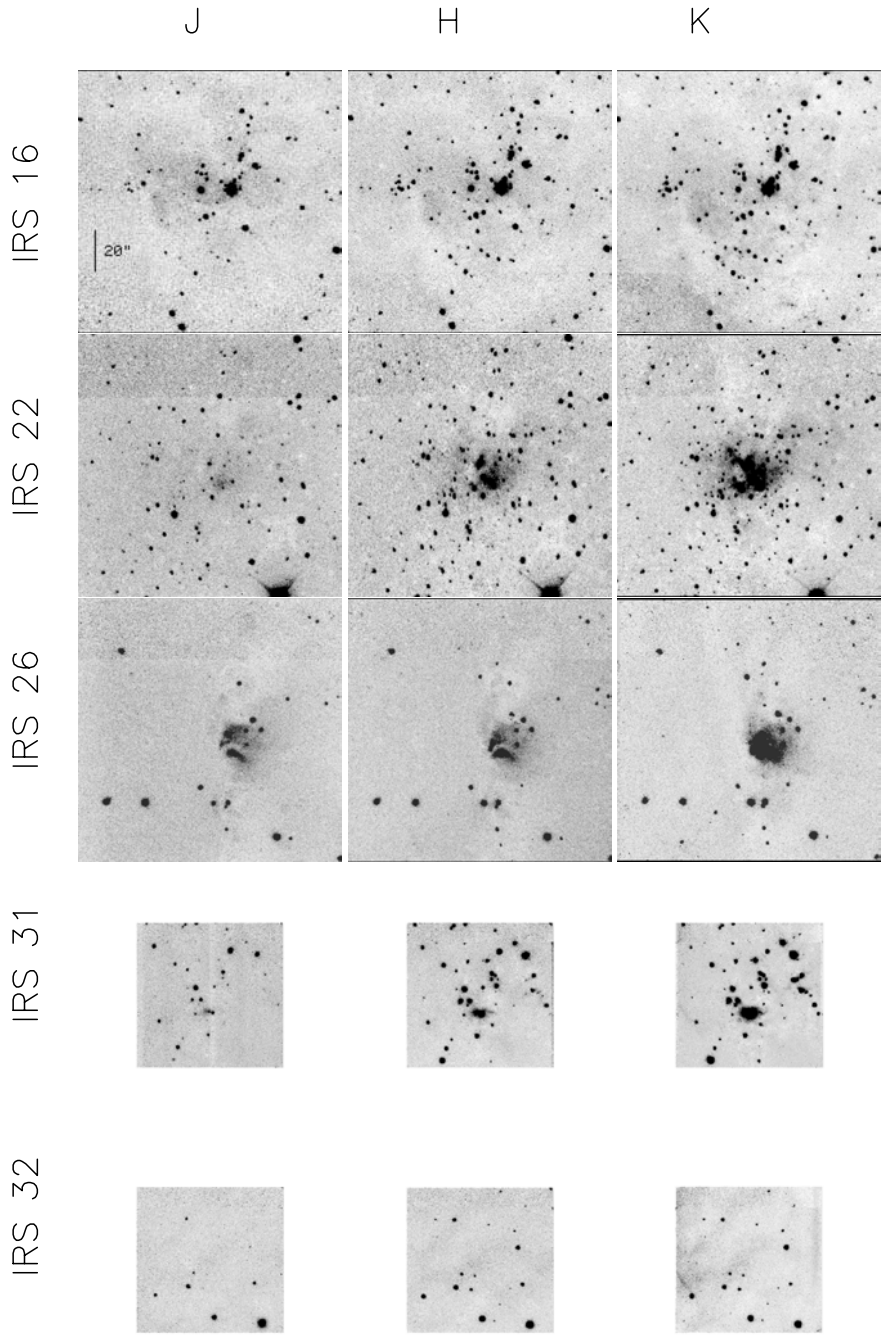

Fig. 2. *J*, *H* and *K* images of all observed fields. Each column refers to the same band (indicated above) and each row refers to the same field (indicated on the left-hand side). North is up and East is left. All frames have been resized such as to share the same scale, which is indicated in the upper left frame.

the most extreme conditions above is always an overestimate; this ensures that in these cases the magnitude "offsets" partially cancel out when deriving the NIR colours.

On each field, the sources' equatorial coordinates were derived as explained in Paper III and are hence calibrated on the HST Guide Star Catalogue (GSC). We estimate that the positional accuracy is $\sim 1''$, although it may be worse towards some of the smaller fields imaged in 1994 due to the smaller number of suitable NIR sources with optical counterparts in the DSS plates.

A total of $\approx$1000 sources have been detected in *K*. Their equatorial coordinates (from the *K*-band frames) and *JHK* magnitudes are listed in Table 5. The final *JHK* images are shown in Fig. 2. For objects undetected in *H* and/or *J*, an upper limit is estimated by examining the magnitude-error diagram of each frame.

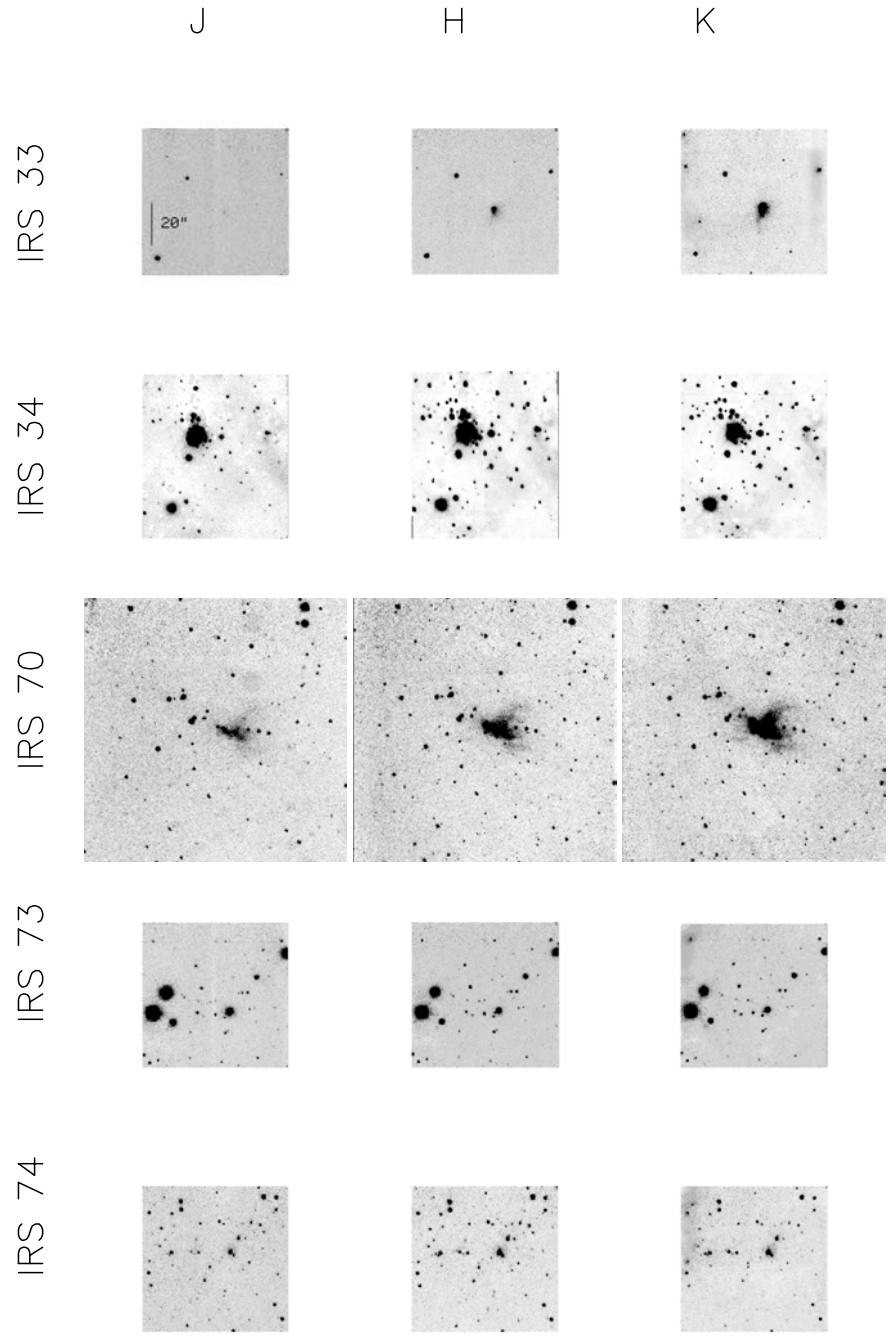

Fig. 2. Continued.

2.3. Continuum mm observations

Some of the fields (see Table 1) were observed at 1.3 mm with the SEST 15-m telescope, sited in La Silla (Chile), during September 1992. The ^{3}He-cooled bolometer of the MPIfR was used as a detector (Kreysa 1990). The beam size is 24″ (HPBW) and the chop throw is 70″. The observing procedure and data reduction are described in Paper III.

3. Results

3.1. Identifying the NIR counterparts

As a first step, we searched for the NIR counterparts of the 10 IRAS sources following the prescriptions given in Paper III. In essence, we retrieved all NIR sources in a 1-arcmin^2 area around the IRAS uncertainty ellipses comparing their positions, colours and NIR fluxes. The true counterparts should lie within the uncertainty ellipse and exhibit a NIR infrared excess and, hence, a very steeply rising λF_λ with wavelength. A detailed analysis of each field follows. The tentatively identified NIR counterparts are listed in Table 2. The NIR sources, when not specified, are referenced by the numbers assigned to them in Table 5.

3.1.1. IRS 16 (IRAS 08438–4340)

The IRAS source coincides with the HII region 263.619-0.533 (Caswell & Haynes 1987), whose centre lies on the

Table 2. Possible NIR counterparts of the IRAS sources.

IRAS source	NIR source	α(2000.0)			δ(2000.0)			K	Identification[a]	Cloud
		h	m	s	°	′	″	(mag)		
IRS 16	90?	08	45	35.4	−43	51	01	9.47	OB,UCHII	D
IRS 22	111	08	50	21.2	−44	30	43	11.41	I	D
IRS 26	15	08	53	09.4	−42	13	08	11.66	I	C
IRS 31	14	08	58	12.8	−42	37	36	9.45	I	C
IRS 32	?	-	-	-	-	-	-	-	?	C
IRS 33	4	-	-	-	-	-	-	11.14	I	C
IRS 34	14?	08	59	28.3	−43	46	04	7.52	OB,UCHII	C
IRS 70	65	08	50	15.9	−44	25	58	11.18	I	D
IRS 73	12	08	55	16.3	−42	43	12	12.03	HAe/Be?	C
IRS 74	24?	08	56	39.3	−47	34	22	13.72	HAe/Be?	C

[a] I: Class I source; OB: young OB star; HAe/Be: Herbig Ae/Be star; UCHII: ultracompact HII region.

south-westerly border of the IRAS uncertainty ellipse. However, the positional uncertainty of the centre should be ∼30″ (the same as that indicated in Haynes et al. 1979). Its FIR colours fulfil the criterion of Wood & Churchwell (1989) for the selection of UCHII regions. The NIR images clearly show an embedded star cluster within the field (see Fig. 2). The IRAS uncertainty ellipse encompasses a small compact group of stars roughly located at the centre of the cluster (see Fig. 3c), the brightest member (our # 90) being also the NIR source reported in Paper I. Our JHK images suggest the presence of an unresolved object close to # 90, designated as # 196. We could successfully separate their brightness through PSF-fitting photometry. Taken at face value, the location of # 90 in the colour-colour diagram (Fig. 3a) is consistent with a main-sequence star earlier than A0 and reddened by $A_V \sim 5$ mag. Based on this, its K flux and the expected distance of the VMR, it is interesting to constrain its spectral type and, hence, to check whether it is the main ionizing source of the HII region. The dereddened K is ∼ 9.0 mag and, assuming a distance modulus of 9.22 mag (d = 700 pc), the absolute K is ∼ −0.2 mag. Adopting the colours of Koornneeff (1983) and the absolute V magnitudes given in Allen (1976), we find that # 90 is consistent with a B0-B5 ZAMS star. Note that increasing the distance would result in an earlier spectral type. Using the relation given by Mezger (1978) and the radio continuum measurement at 4.85 GHz from the Parkes-MIT survey (see, e.g., Griffith & Wright 1993), we can estimate the number L'_c of ionizing photons absorbed by the gas. For S_ν = 2 Jy and assuming T_e = 10000 K, we get $L'_c \sim 8.7 \times 10^{46}$ s^{-1} which is consistent with a B0 ZAMS star (Panagia 1973). Also the bolometric luminosity of the IRAS point source (see Table 3) is typical of a ZAMS star of B1-B2 spectral type (Panagia 1973). Thus, # 90 is likely to be the main ionizing source of the HII region. In Paper I, photometry at L and M performed on the position of # 90 with a single channel detector (15″ aperture) is reported. The L value, dereddened with the Rieke & Lebofsky (1985) law for A_V = 5 mag, is ∼8.6 mag, again largely compatible with photospheric emission from a B0-B5 star. However, as shown in Fig. 3b, the flux in the M band appears to be somewhat higher than allowed by any possible photospheric contributions. This also suggests that the counterpart of the IRAS source must lie within the uncertainty ellipse, not far from the (projected) location of # 90. One possibility is cold circumstellar matter associated with # 90 itself and is meant above. Source # 123, which has the colours of a Class I protostar and a steeply rising NIR flux (see Fig. 3b) should be discarded since it lies outside the ellipse. The only other possibility is an object close to # 90, either a UCHII region or a Class I source. Sources # 100 and # 196 meet this requirement, exhibit a NIR excess (see Fig. 3a) and have rising SEDs in the NIR (see Fig. 3b). They are also the brightest NIR objects within the ellipse after # 90. Hence, they are both good Class I candidates and alternative to # 90 as counterparts of the IRAS source.

3.1.2. IRS 22 (IRAS 08485-4419)

The field towards IRS 22 discloses a nice example of an embedded star cluster (see Fig. 2), whose centre falls within the IRAS uncertainty ellipse (see Fig. 4c). Our source # 111 is clearly the one found by Liseau et al. (1992) through single channel photometry and, as shown in Fig. 4b, has a steeply rising NIR flux with wavelength which smoothly joins the L and M values given in Paper I. In the colour-colour diagram (Fig. 4a) it is located slightly below the reddening band, near the cross-like symbol marking an A0 V star reddened by A_V∼ 30 mag. Thus, it is not clear if its apparent colour excess is real or due to photometric errors. Furthermore, Fig. 4 does not allow to exclude a contribution to the FIR flux from other objects within or close to the uncertainty ellipse which exhibit both a colour excess and steep SEDs in the NIR. Pending further confirmations, we tentatively identify source # 111 as the "main" counterpart of IRS 22.

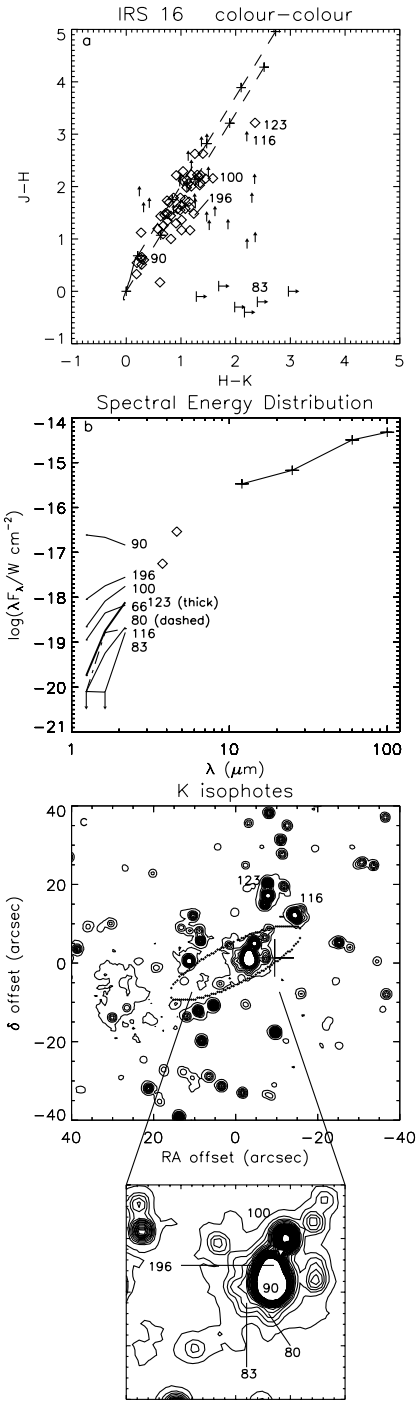

Fig. 3. a) Colour-colour diagram; **b)** SEDs of some of the possible NIR counterparts of IRS 16 (along with the fluxes in the *L*, *M* and IRAS bands); and **c)** contour plot of the *K* flux around the IRAS uncertainty ellipse (dotted line). Contours are in steps of $\sim 1\sigma$ from $\sim 1\sigma$. The large cross marks the location of the HII region 263.619-0.533. The small lower box is a close-up of the central $20'' \times 20''$ region. The solid line in the colour-colour diagram marks the locus of main sequence stars (Koornneef 1983), whereas the dashed lines are the reddening law according to Rieke & Lebofsky (1985); 10 mag intervals of A_V are indicated by crosses. Data points on the right of the two dashed lines represent sources with an intrinsic NIR excess. Upward arrows indicate lower limits in $(J - H)$ and vertical segments with rightward arrows indicate sources with only upper limits at *J* and *H*. The diamonds in box **b)** are the *L* and *M* values quoted in Paper I.

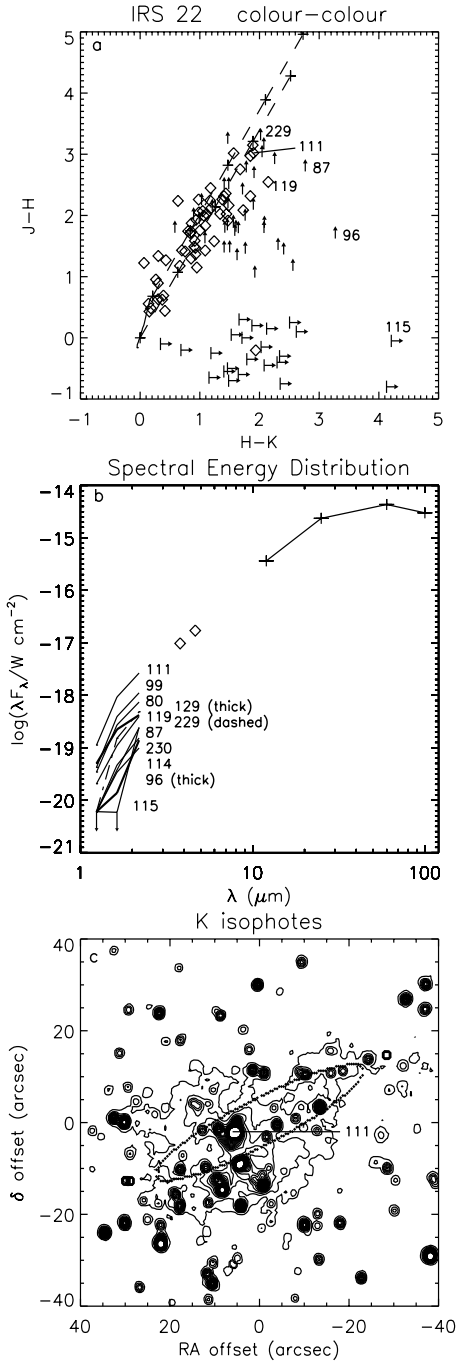

Fig. 4. Same as Fig. 3, but for IRS 22.

3.1.3. IRS 26 (IRAS 08513–4201)

The IRAS source coincides with a nebula (also known as BBW 192E) which appears bipolar at NIR wavelengths along a northeast-southwest orientation (see Fig. 2 and Fig. 5c). At optical wavelengths, an elongated structure on a southeast-northwest direction borders on the NIR emission, north of it. A comprehensive discussion of optical, NIR, MIR and mm data (including NIR polarimetry) is presented in Burkert et al. (2000). However, their NIR imaging data are limited to the *H* and K' bands and appear less deep than our own, so the

JHK photometry we carried out complements their study. We must note that a comparison between their photometry and ours unveiled a systematic difference, with their measurements brighter of ∼1 mag in K' and H. We could not find any flaws in our photometry; on the contrary, we could reproduce quite well the values from single channel photometry given in Paper I using a synthetic aperture, whereas Burkert et al. (2000) claim that they obtain somewhat higher fluxes with the same technique. The 1.3-mm continuum map (Fig. 2d of Burkert et al. 2000) shows a cometary structure which is peaked towards the NIR nebula. The IRAS uncertainty ellipse clearly encompasses the mm peak and the southwestern lobe of the nebula (see Fig. 5c). Burkert et al. (2000) suggest our object # 15 (their 25), embedded within the nebula, as the energy source of IRS 26. The extended emission in the NIR is interpreted as dust scattering and the NIR polarimetry shows that # 15 is very likely the major illuminator. Indeed, its location on the colour-colour diagram (Fig. 5a) and its rising SED (Fig. 5b) meet our prescriptions. According to this picture, # 15 is located slightly off the uncertainty ellipse because IRAS traces the heated dust rather than the heating star. Our object # 23 (18 of Burkert et al. 2000) has similar properties as # 15 and lies within the ellipse, but its location far from the nebula (see Fig. 5c) suggests that it is not the main contributor to the FIR flux, although it could account for a significant fraction of it. Hence, the analysis of Burkert et al. (2000) and our own NIR data both point to source # 15 as the counterpart of the IRAS source.

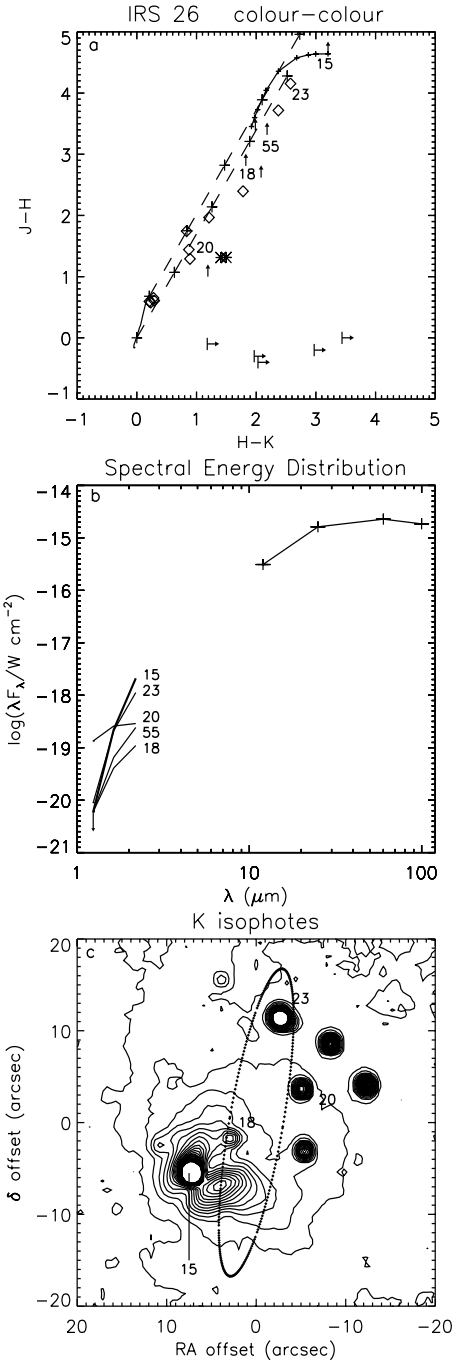

Fig. 5. Same as Fig. 3, but for IRS 26. The asterisks in **a)** mark the colours of different parts of the imaged nebula, whereas the curved line represents a $\tau_0 \times \lambda^{-4}$ scattering law drawn by varying τ_0 (see Sect. 4.2 of Paper III).

3.1.4. IRS 31 (IRAS 08563–4225)

Despite the smaller field of view, the NIR images clearly show a stellar cluster towards IRS 31 (see Fig. 2). Source # 14 is associated with diffuse emission and is roughly located at the centre of the IRAS uncertainty ellipse (Fig. 6c), exhibits a marked NIR excess (Fig. 6a) and has a steeply rising SED (Fig. 6b). There are few doubts, if any, that it is the counterpart of the IRAS source. It coincides with IRS31/2 of Paper I, although ∼1 mag fainter in H and ∼2.5 mag fainter in J than the single channel photometry. This means that diffuse emission was collected within the 15″ aperture of the photometer, probably due to radiation scattered by dust surrounding source # 14. Although much brighter (which is puzzling), our # 2 coincides in position with IRS31/3 of Paper I and, despite its steeply rising SED in the NIR (Fig. 6b) it apparently does not exhibit a NIR excess (even if it is heavily reddened; Fig. 6a) and lies outside the ellipse (Fig. 6c). Other fainter NIR objects within or very close to the ellipse display or may display a NIR excess (e.g., # 30, 75, 34), as well, nevertheless # 14 appears as the NIR counterpart.

3.1.5. IRS 32 (IRAS 08575–4330)

The NIR images do not show any good counterpart candidates for IRS 32 (see Fig. 7). Too few stars lie within the (small) field of view for the astrometry, so equatorial coordinates were determined based on the coincidence between the photometry of our source # 4 and IRS 32/1 of Paper I, assuming that the position given in Paper I for the latter is reliable enough. It is puzzling that source # 1, even brighter than # 4 (IRS 32/1), was apparently not found through the single channel photometry. IRS32/2 roughly coincides in position with # 10, which is ∼1 mag fainter in K.

We must note that the IRAS flux at 100 μm is quoted in the PSC as an upper limit. Furthermore, the global picture of the field is somewhat reminiscent of IRS 66 (see Paper III): both sources exhibit a FIR flux decreasing from 12 to 25 μm and

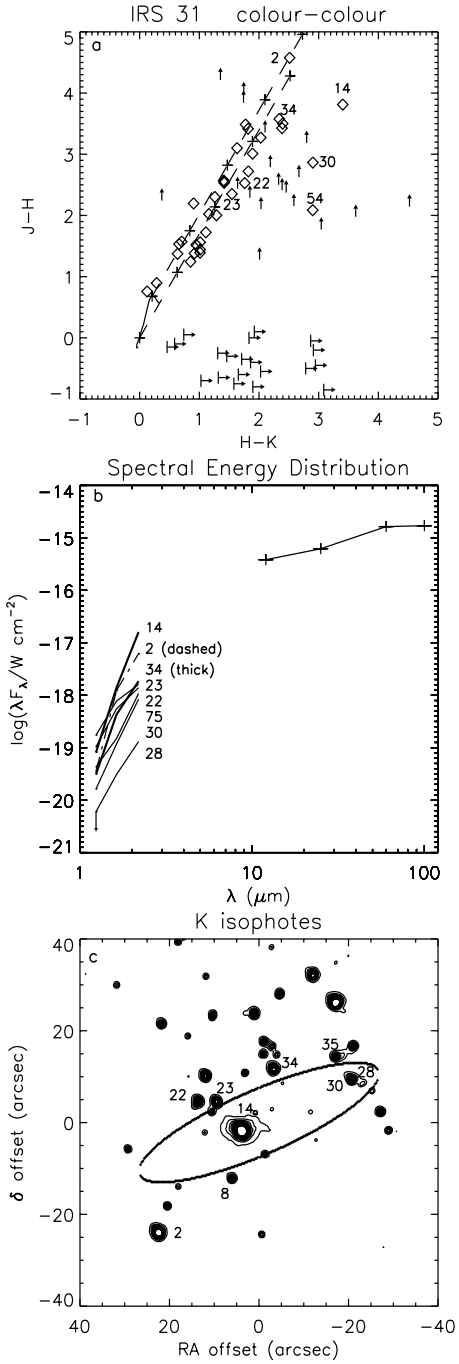

Fig. 6. Same as Fig. 3, but for IRS 31.

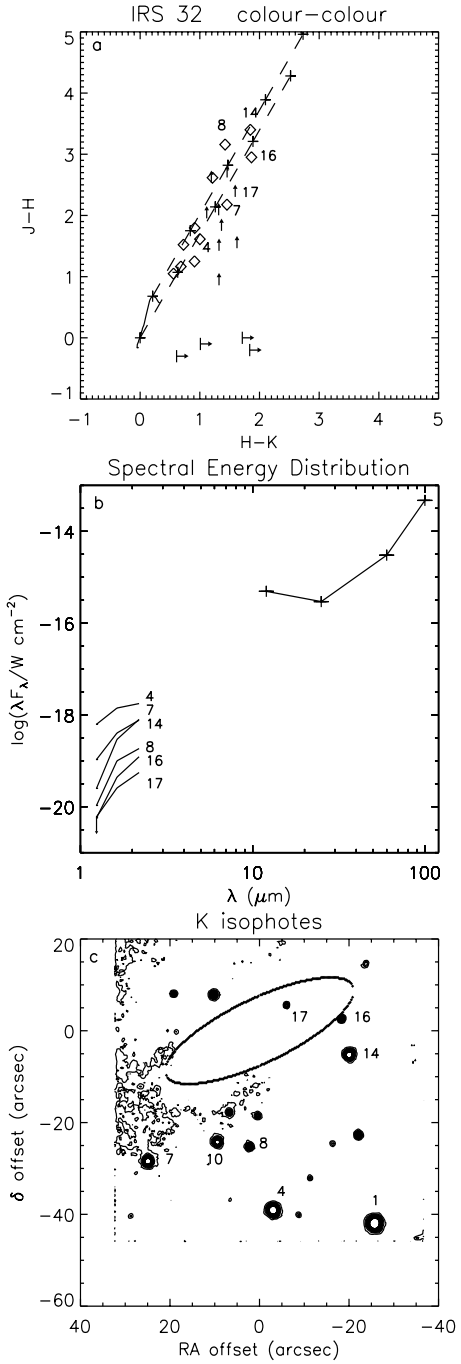

Fig. 7. Same as Fig. 3, but for IRS 32.

then increasing longward and both are located in close proximity to an HII region (RCW 32 and RCW 36). In the case of IRS 66, we found a possible NIR counterpart ∼ 40″ from the ellipse centre, concluding either that an ellipse displacement arouse due to confusion with the HII region emission, or that the real counterpart is fainter than the completeness limit. Actually, a look at the IRAS maps towards IRS 32 indicates that the FIR emission in the area is largely affected by that of the HII region RCW 36 and of its associated IRAS point source (see IRS 34, below). Hence, the bolometric luminosity given in Paper I is overestimated and just like IRS 66, the counterpart could either lie off field (it would be so for IRS 66 had it been imaged with the same field of view as IRS 32) or be too faint. In Paper I it is also reported that the maximum of CS(2–1) emission is offset by (−50″,−50″). If the actual bolometric luminosity is much lower, then the IRAS source falls in a region of the luminosity vs. mm-flux diagram (see Fig. 17) occupied by lower mass young stellar objects which are either isolated or in small groups. Hence, both deeper (and on a larger field) NIR imaging and mm (line and continuum) maps of the region are needed to settle the point.

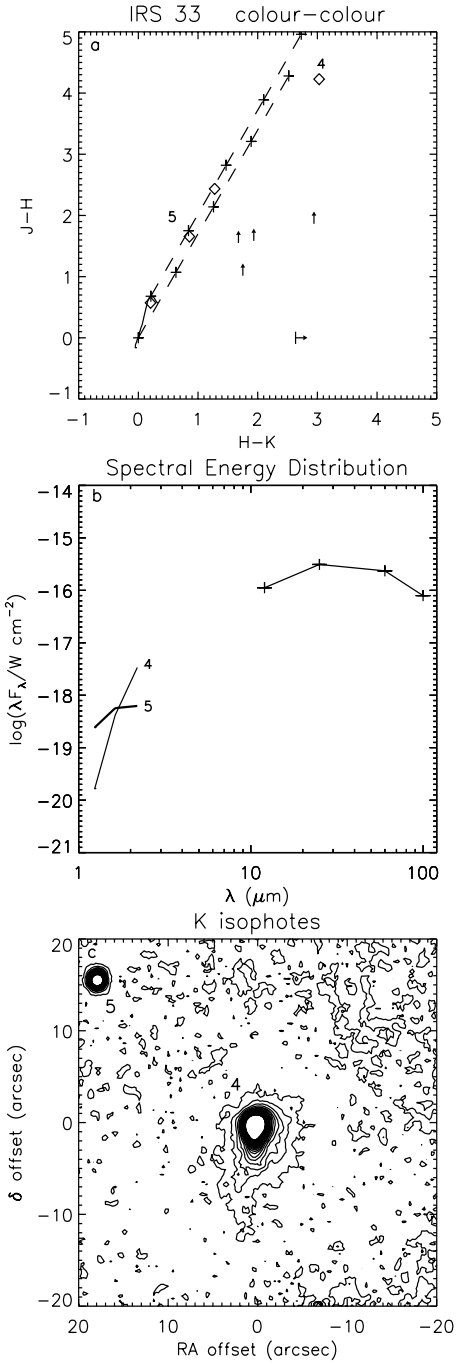

Fig. 8. Same as Fig. 3, but for IRS 33.

3.1.6. IRS 33 (IRAS 08576–4314)

Too few stars are imaged within the field (see Fig. 2) and this does not allow astrometry. However, undoubtedly source # 4, also associated with diffuse emission, is the NIR counterpart of the IRAS source (see Fig. 8). The photometry coincides with that quoted in Paper I. It represents a remarkable example of an isolated young star object likely classifiable as a Class I source.

3.1.7. IRS 34 (IRAS 08576–4334)

This IRAS source was discarded as a Class I candidate in Paper I, however we include it in the present sample due both to the presence of a star cluster and to its association with an HII region (265.151+1.454 of Caswell & Haynes 1987; also known as RCW 36 and BBW 217). Its FIR colours are typical of a UCHII region, according to the criterion of Wood & Churchwell (1989). The stellar cluster is well evident in our NIR images (see Fig. 2) around the northernmost of the two brightest sources. Although this latter is most likely the ionizing source of the HII region, lying only a few arcsec west of the radio continuum peak, Fig. 9c clearly shows that the IRAS uncertainty ellipse is offset south of it. Note that sources # 68 and # 14 are saturated, at least in the K image, but due to their remarkable brightness we can safely rely on the single channel photometry by Braz & Epchtein (1982). In fact, the only other bright source which falls into the photometer aperture, # 59, does not appear saturated in our images and is ∼1 mag below the JHK values given by these authors (their source 2). Hence, it cannot affect the photometry more than ∼0.5 mag. As for the counterpart of the IRAS source, # 14 borders the eastern edge of the uncertainty ellipse and seems to exhibit a NIR excess. However, its SED appears to flatten in the L band (see Fig. 9b). Although emission from a circumstellar envelope could result in a second peak at FIR wavelengths, we may consider also source # 36, which lies within the ellipse, has a steeply rising SED and seems to show a NIR excess. Sources # 39 and # 71 are surrounded by diffuse emission at K (see Fig. 9c); whereas # 71 does not appear to exhibit a NIR excess and is located slightly off the ellipse, # 39 may have a NIR excess (see Fig. 9a) and its SED is rising (see Fig. 9b).

So, a NIR counterpart of the IRAS source cannot be confidently identified, but some conclusions can be drawn based on FIR observations at 58 μm and 150 μm by balloon-borne telescope. Verma et al. (1994) find two peaks in these bands (their S1 and S3) north and south of the IRAS uncertainty ellipse, whose locations are shown in Fig. 9c by asterisks. They do not coincide with any of the imaged NIR sources. These could be UCHII regions, which usually are undetected at NIR wavelengths. However, the angular resolution is 1.5′ and the authors claim that given positions are accurate within ∼1′. Hence, they could actually correspond to # 68 and # 14 themselves. The derived bolometric luminosity is 1.5×10^4 $L_\odot$ for the northern source and 1.7×10^4 $L_\odot$ for the southern one.

It is remarkable not only that at least one prominent FIR source is located off the cluster centre, but also that a detected H_2O maser (the westernmost cross in Fig. 9c), whose position is given by Braz & Scalise (1982), is offset from it. Since the cluster appears more evolved than those studied in Paper IV (its members are reddened with very few ones exhibiting NIR excess), all these objects trace very different stages in star formation and evolution, nevertheless they coexist in a small sky area. Then, we can speculate that sequential star formation, induced by the expanding HII region, is currently taking place south and west of the cluster, or behind it. Indeed, a few mm observations confirm that a molecular core where star formation may be in progress lies probably behind the HII region. In fact, in Paper I it is reported that intense CS(2–1) emission (1–4 K) towards the IRAS source forms a ridge in a southeast-northwest direction, whereas intense $C^{18}O$(2–1) at a ∼5 K level

has been detected 40″ west of the radio peak (Zinchenko et al. 2000).

It is useful to try a spectral classification of source # 68 in the same way as done for IRS 16. Its location in the colour-colour diagram is consistent with that of a main sequence star earlier than A0, reddened by $A_V \sim 10$ mag. Using the colours of Koornneef (1983) and the absolute magnitudes given by Allen (1976), and assuming a distance modulus of 9.22 mag (700 pc) we find that the dereddened K flux may be accounted for by a main sequence star between O5 and B0. Verma et al. (1994) compute $N'_{\rm C} \sim 2.4 \times 10^{48}$ photons s^{-1}, which may be supplied by one O8 star or two O9 stars of zero age main sequence. These could yield a bolometric luminosity of ~6–9 $\times 10^4$ $L_\odot$ (Panagia 1973), consistent with the total far infrared luminosity of 5.7×10^4 $L_\odot$ derived by Verma et al. (1994). This indicates that # 68 is indeed the main ionizing source of RCW 36. Whether the southernmost FIR peak coincides with source # 14 or not, its $L_{\rm bol}$ (estimated to be 1.7×10^4 $L_\odot$ by Verma et al.) would suggest an earlier than B1–B0 star of zero age main sequence (Panagia 1973). Hence, RCW 36 is a site of active massive star formation.

3.1.8. IRS 70 (IRAS 08485–4414)

This source was not included by Lorenzetti et al. (1993) in their catalogue, mainly due to lack of mm-line observations which could establish its association with the VMR. However, its location appears to overlap a small cloudlet visible in both ^{12}CO and ^{13}CO(1–0) on the maps of Yamaguchi et al. (1999; see Fig. 1). IRS 22 lies towards the same cloudlet, south of IRS 70. The IRAS uncertainty ellipse encompasses a diffuse nebulosity with a small group of point-like objects inside showing large reddening and NIR excess (see Fig. 10c). The brightest source, # 65, has a steeply rising SED and is probably the counterpart of the IRAS source. Hence, IRS 70/# 65 actually meets the requirements of Liseau et al. (1992) and should be considered, in their words, a *bona fide* Class I source associated with the VMR.

Note that it has been also suggested that IRAS 08485–4414 is a Galaxy (Yamada et al. 1993; Weinberger et al. 1995), which appears very unlikely, as clearly shown by our NIR images and photometry.

3.1.9. IRS 73 (IRAS 08534–4231)

The two sources found by Lorenzetti et al. (1993) through single channel photometry are our # 10 (IRS 73/1) and # 12 (IRS 73/2). As noted by those authors, IRS 73/1, which lies outside the IRAS uncertainty ellipse, is a reddened stars. IRS 73/2 is located within the ellipse and coincides with PRHα 261. Its NIR colours (see Fig. 11a) are consistent with an earlier than A0 star, with little reddening and apparently no NIR excess. Hence, an evolved Herbig Ae/Be star. Single channel L-photometry from Paper I is shown in Fig. 11b for both IRS 73/1 and IRS73/2. There are little doubts that L is photospheric in origin for IRS 73/1, whereas increasing towards IRS 73/2. This suggests that the counterpart must be located within the

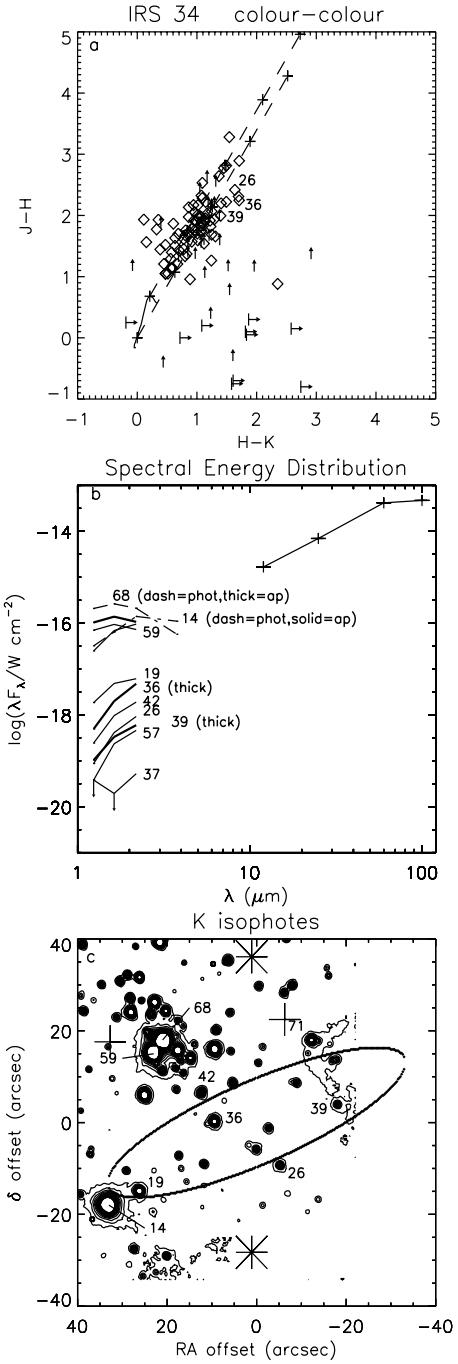

Fig. 9. Same as Fig. 3, but for IRS 34. The easternmost cross in **c)** marks the location of the radio peak associated with the HII region RCW 36, whereas the westernmost one is at the position of the H_2O maser (see text). The two asterisks are at the location of the FIR peaks found by Verma et al. (1994). In box **b)**, the SEDs of # 14 and # 68 from the photometry of Braz & Epchtein (1982) are drawn as dashed lines, those from our own measurements as solid (# 14) and thick (# 68) lines.

15″-diameter aperture of the photometer, very close to IRS 73/2 (# 12), which was argued in Paper II. We do not find any suitable candidates other than # 12 for the counterpart. Either it is extremely faint at NIR wavelengths, or the IRAS emission arises from a circumstellar envelope associated with # 12, but detached from it, such as to yield a double-peaked spectrum.

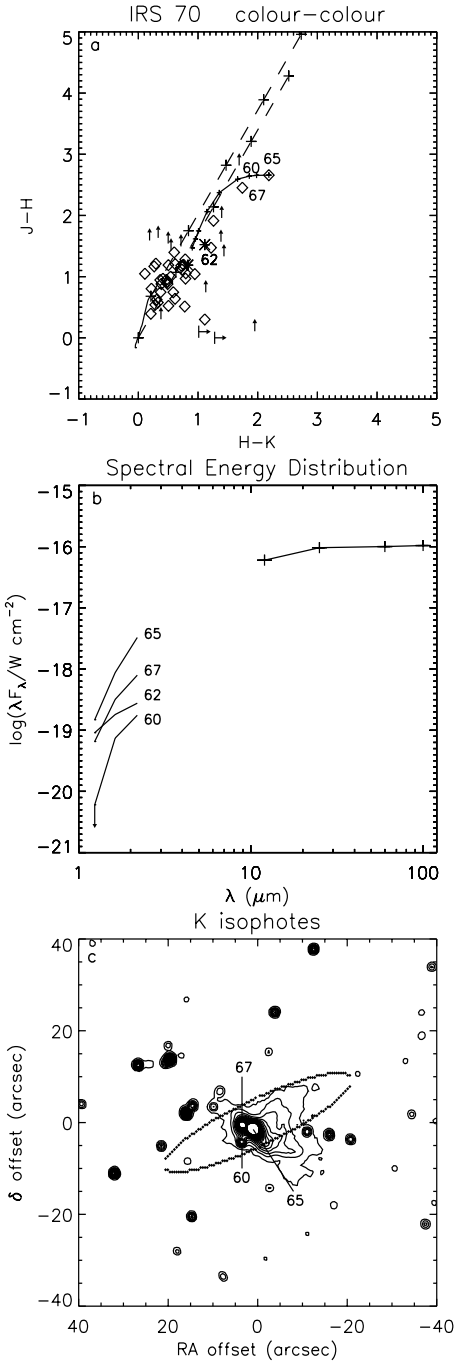

Fig. 10. Same as Fig. 3, but for IRS 70. The asterisks in **a)** mark the colours towards 2 different parts of the observed nebula, whereas the curved line represents a $\tau_0 \times \lambda^{-4}$ scattering law drawn by varying τ_0 (see Sect. 4.2 of Paper III).

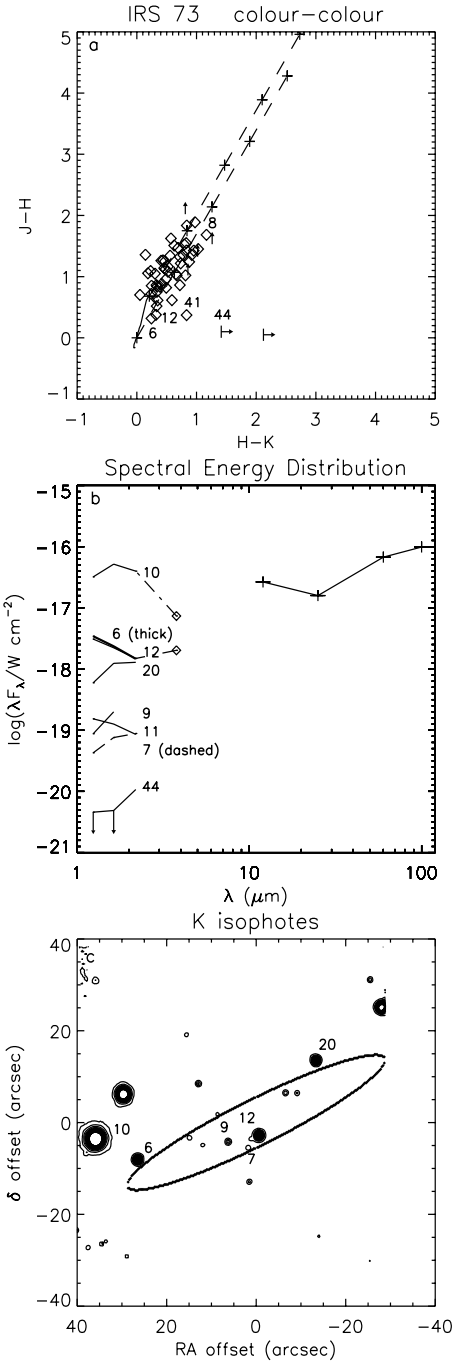

Fig. 11. Same as Fig. 3, but for IRS 73.

3.1.10. IRS 74 (IRAS 08549–4722)

No NIR sources were found by Lorenzetti et al. (1993) up to $K \sim 12.5$ mag towards IRS 74. However, they found 1.3-mm continuum emission suggesting the source is actually a Class I candidate. The IRAS uncertainty ellipse (Fig. 12c) encompasses our source # 24, the brightest in the field, which is surrounded by diffuse emission. Its location in the colour-colour diagram is consistent with an earlier than A0 star reddened by $A_V \sim 10$ mag and exhibiting a small degree of NIR excess. Then, it is likely to be a Herbig Ae/Be star. Source # 25, within the ellipse, has a steeply rising SED and seems to show some NIR excess. However, in this case too, it is difficult to discriminate between FIR emission from a hardly detectable Class I object or a detached circumstellar envelope around the (possible) Herbig Ae/Be star.

3.2. Comparison with the results of Papers I and II

The NIR counterparts we find for the 7 IRAS sources (IRS 22, IRS 26, IRS 31, IRS 32, IRS 33, IRS 73, IRS 74) listed in the catalogue of Papers I and II as (VMR-)Class I sources are

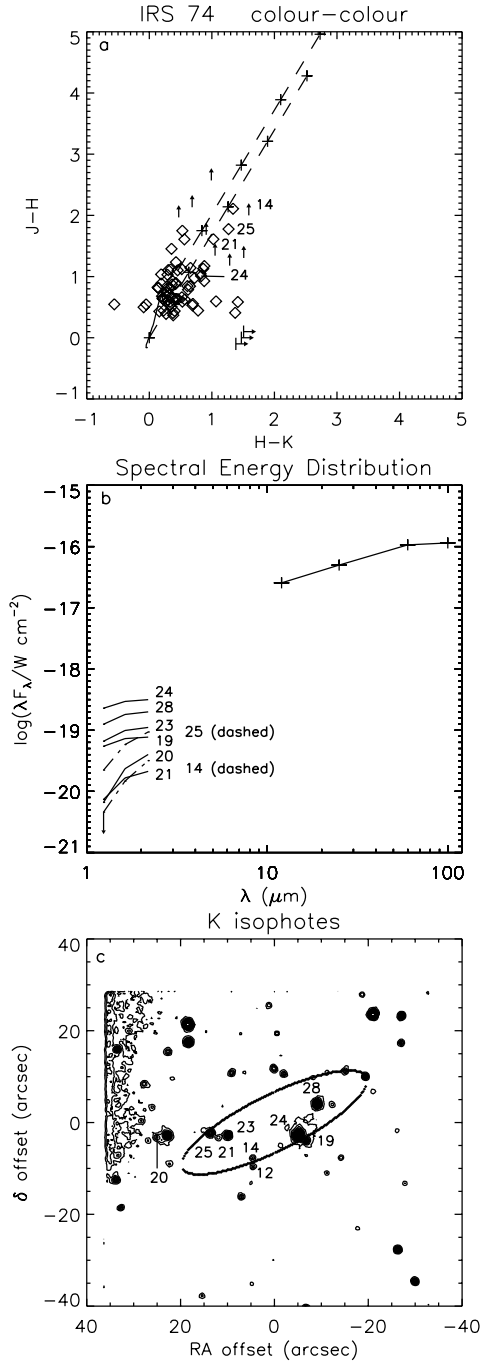

Fig. 12. Same as Fig. 3, but for IRS 74.

generally in agreement with those reported in these papers to have been detected with the single channel NIR photometer. As for IRS 74, the authors did not observe any emission at a $K < 12.5$ level, whereas the identification of IRS 32 in Paper I appears doubtful (and no good candidates have been found in our images). Of the remaining 5 sources, the NIR photometry quoted for IRS 26 refers to the nebular emission illuminated by our object # 15, which is a very reddened (proto-)star and, in its own right, is to be considered as the real counterpart. In the case of IRS 33, which is an isolated young stellar object, our HK photometry coincides with the values given in Paper I within 0.1 mag (actually, for the J band our measurement agrees with the quoted lower limit). Towards IRS 22, IRS 31 and IRS 73, our JHK magnitudes are larger than reported in Papers I and II (up to 0.5 mag, with the exception of IRS 31 in the H and J bands; see Sect. 3.1.4), but this is consistent with the greater flux falling in the 15″ aperture of the single channel photometer due to diffuse emission and source crowding.

3.3. Continuum mm data

We used the 1.3-mm fluxes, when available, in order to estimate the masses of circumstellar envelopes, as explained in Paper III. These are listed in Table 3 along with the bolometric luminosities. The results on envelope masses should be taken with caution; consider, e.g., the case of IRS 26: the 1.3-mm measurement was carried out towards the IRAS source. But this, in turn, coincides with the mm peak of the molecular core (indeed, our value of 0.5 Jy agrees quite well with that of 0.6 Jy found by Burkert et al. 2000 at peak), so the emission traces the latter rather than the circumstellar environment. Anyway, if we assume that the values given in Table 3 are rough estimates of the envelope masses, we must note that these are generally lower (0.2–5.1 $M_\odot$) than those found towards the sources studied in Paper III (0.2–15 $M_\odot$). Excluding IRS 16, IRS 32 and IRS 34, the bolometric luminosities, for a protostellar scenario, would be indicative of masses in the range 3.5–6 $M_\odot$ according, e.g., to the model of Palla & Stahler (1993) with a standard accretion rate 10^{-5} $M_\odot$ yr^{-1}. Hence, the envelope/star mass ratios would vary from ~ 1 down to $\ll 1$. Table 3 also lists the bolometric luminosities of IRS 16, IRS 34 and IRS 70, for which no measurements at 1.3 mm are available. In these cases we extrapolated the latter assuming grey body emission longward of 100 μm with an emissivity $\sim \lambda^{-1.5}$ and $T = 40$ K, which in general gives a good approximation of the mm emission towards the other fields. The $L_{\rm bol}$ estimated for IRS 34 (4.9×10^4 $L_\odot$) in this way compares well with that given by Verma et al. (1994), i.e. 5×10^4 $L_\odot$.

3.4. Reflection nebulae

As already found towards many of the 12 fields discussed in Paper III, in general diffuse emission is evident around the NIR counterparts of the 10 IRAS sources studied herein (see Fig. 2 and Figs. 3c to 12c). The most remarkable instance is that of IRS 26, but also IRS 70 shows a clear pattern of nebular emission, whereas the NIR counterparts of IRS 31 and IRS 33 shine through nebulosities. In Paper III this diffuse emission was attributed to scattering from the dust particles close to the young stellar objects. Burkert et al. (2000) confirm the picture in the case of IRS 26 and their NIR polarimetry allows to identify our source # 15 as the illuminator.

The results of Burkert et al. (2000) are quite useful as a benchmark for the simple model presented in Paper III for deriving the NIR colours of reflection nebulae from those of the illuminator (see Sect. 4.2 in the paper). Simply assuming an isotropic $\sim\lambda^{-4}$ scattering, we can construct the locus of theoretical colours (starting from the illuminator data point) in a $H-K$ vs. $J-H$ diagram. This is shown in Fig. 5a (the solid line

extending leftward of # 15) along with the colours of the south-western and north-eastern lobes of the nebula (marked by asterisks). These have been determined by integrating the emission in K down to a level of a few sigmas, and then using the IRAF tasks *geomap* and *geoxytran* to compute the spatial transformations between the JHK frames and define the same polygonal aperture on the sky. Since the illuminator and the nebula are differentially extincted, the scattering locus has to be shifted back along the reddening vector until overlapping the observed nebular colours. This also allows an estimate of how much the illuminator is extincted with respect to the nebula (i.e., just the length spanned by the shift). In the case of IRS 26, it is evident that, if # 15 is indeed the illuminator, according to our simple model it must have an $A_V \sim 30$ mag larger than the nebula. When dereddened by such an amount using the Rieke & Lebofsky (1985) law, the illuminator becomes at least 2 mag brighter than the integrated diffuse emission, as it has to be (the nebula cannot be more luminous than its illuminating source). We have to note that the nebula is ∼1.5 mag brighter in K than in H and ∼1.3 mag brighter in H than in J. The same was found in Paper III for a few regions and attributed partly to the rising SED of the illuminator and partly to the extinction. We do not think, as suggested by the referee, that line contamination may be important in determining the trend. E.g., when subtracting the continuum contribution from narrow-band (centred at the 2.12 μm line of H_2) images of the fields examined in Lorenzetti et al. (2002), this kind of diffuse emission disappears, indicating that the line contribution is negligible.

We also determined the NIR colours for 2 different parts of the diffuse emission towards IRS 70 and indicated them (with asterisks) in Fig. 10a. It is evident that, when shifted along the reddening law, the scattering locus from # 65 intercepts both nebular data points. The differential extinction in the visible would be a few mag to ∼10 mag. When dereddened by $A_V = 10$ mag, # 65 becomes brighter than the nebula in all three bands of at least 1 mag. Hence, it is consistent with being the illuminating source of the close-by dust structure.

It is interesting to remark the presence of a dark lane between the two lobes of the nebula towards IRS 26, close to the NIR counterpart (see Fig. 2 and Fig. 5c), which is suggested as the signature of a circumstellar disk, seen edge-on, by Burkert et al. (2000). The disk, when scaled to our assumed distance, would have a diameter ∼1400 AU. This morphology is reminiscent of IRS 20 in Paper III (see Fig. 8c there), where a deeply embedded NIR source lies within a dark lane between the 2 lobes of a roughly bipolar nebula. An edge-on disk would also explain the much higher extinction towards the illuminator with respect to the nebula we find in both regions by comparing their NIR colours. Hence, the picture put forward by Burkert et al. (2000) for IRS 26 is worth being further investigated in the case of IRS 20 as well.

3.5. Clustering

We evidence the clustering of stars towards the IRAS sources using the same techniques as in Paper IV. First, for each of the K images shown in Fig. 2 we counted all sources found in 20″ × 20″ squares displaced of 10″ (along both right ascension and declination) from each other (i.e., a Nyquist sampling interval). We grouped together all these surface density bins from the 10 fields and added them to the ensemble of those from the 12 fields of Paper IV. Then, we updated the frequency distribution of star counts which is shown in Fig. 6 of Paper IV for the 12 fields. We still find that, whether the counting includes sources above the limiting magnitude or not, the distribution is approximated by a curve which is a Poissonian around the peak, but with a marked excess of counts in the wing. In Paper IV we interpreted this as evidence of a real star clustering towards most of the fields. Although we have found slightly smaller mean values for the new Poissonian curves than those in Paper IV, which should give an estimate of the average surface density of field stars, for this latter we will assume the same values as in Paper IV, i.e., ∼2 stars per unit cell (20.0 stars arcmin^2) or ∼1 star per unit cell when excluding detections with $K > 15.5$ mag (i.e., above the completeness limit). Contour maps of the star surface density in 8 out of 10 K-band images are shown in Fig. 13. We limited the counting to detections with $K < 15.5$ mag (i.e., below the completeness limit) in order to remove small structures due to extremely faint

Table 3. Bolometric luminosities and circumstellar envelope masses derived from the dust emission in the continuum at 1.3 mm.

Source	$L_{\rm bol}$ ($L_\odot$)	$M_{\rm env}$ ($M_\odot$)
IRS 16[a]	4.8×10^3	-
IRS 22	3.6×10^3	5.1
IRS 26	2.2×10^3	3.0
IRS 31	1.9×10^3	2.8
IRS 32	$< 4.8 \times 10^3$	0.3
IRS 33	1.5×10^2	0.4
IRS 34[a]	4.9×10^4	-
IRS 70[a]	$< 1.2 \times 10^2$	-
IRS 73	1.0×10^2	0.2
IRS 74	1.3×10^2	0.7

[a] mm flux inferred as explained in the text (only for $L_{\rm bol}$).

Table 4. Physical parameters of the identified star clusters and groups.

Source	Size ($2R$) (pc)	I_c	Peak surface density (pc^{-2})	Volume density (pc^{-3})
IRS 16	0.30	26 ± 1	3.4×10^3	5.9×10^3
IRS 22	0.35	38 ± 1	3.4×10^3	2.1×10^3
IRS 26	0.13	4 ± 0	1.2×10^3	1.4×10^4
IRS 31	>0.20	>15	2.4×10^3	$< 1.6 \times 10^4$
IRS 34	>0.20	>58	4.8×10^3	$< 2.6 \times 10^4$
IRS 70	0.07[a]	4 ± 0	1.2×10^3	1.4×10^4
IRS 73	0.09[a]	7 ± 1	1.2×10^3	7.3×10^3

[a] from the maps where only sources with $K < 15.5$ mag are counted.

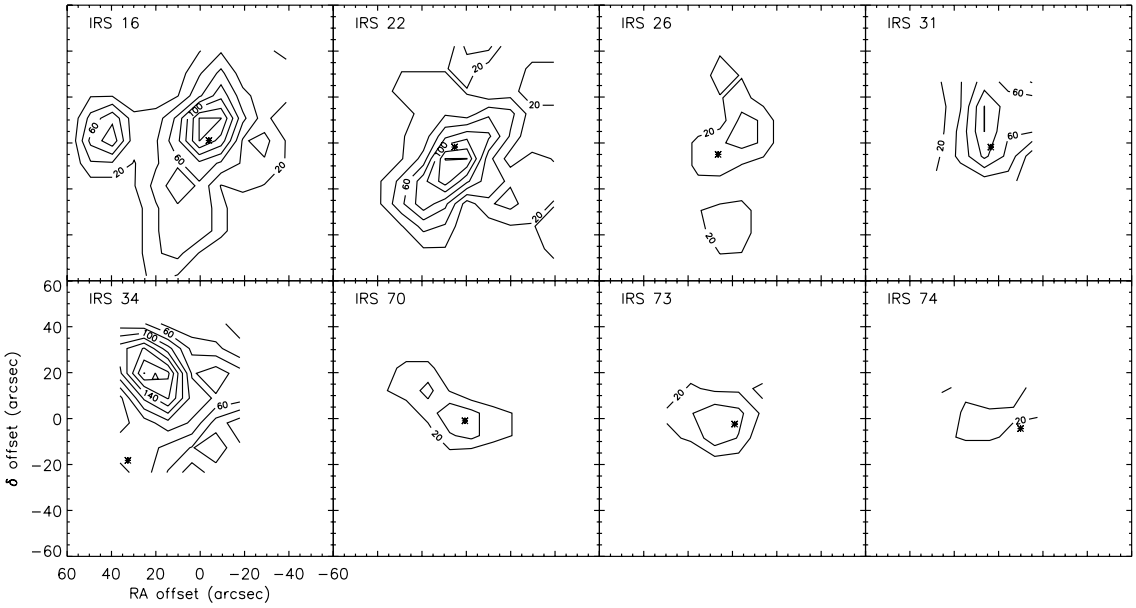

Fig. 13. Contour maps of stellar surface density (from K images) obtained by counting sources in square bins of $20'' \times 20''$, offset by $10''$. Right Ascension and Declination are arcsec offsets from the IRAS uncertainty ellipse centre. The lowest contour amounts to 20 stars arcmin^{-2}, roughly the mean field star density, and the steps are 20 stars arcmin^{-2}, corresponding to intervals of $\sim 2\sigma$. Asterisks mark the locations of the IRAS counterparts identified in the text. The open triangle towards IRS 34 indicates the location of IRS 34/# 68, the ionization source of the associated HII region, which may be part of the IRAS source itself (see the text).

sources which appear somewhat doubtful. Note that IRS 16, IRS 22, IRS 31 and IRS 34 clearly exhibit star clustering well above a *mean sky* $+3\sigma$ level. However, traces of smaller source grouping are present towards the other fields in the figure, as well.

As described in Paper IV, we also determine the radial surface density of K sources, $n(r)$, for the 8 fields of Fig. 13. We do that simply counting the objects with $K < 15.5$ mag in concentric annuli $6''$ wide centred on the identified NIR counterparts (on # 68 in the case of IRS 34). The obtained distributions are shown in Fig. 14; the error bars mark a 1σ Poissonian fluctuation in the counts. All fields exhibit some degree of star clustering towards the NIR counterpart and, in particular, IRS 16, IRS 22 and IRS 34 are associated with relatively rich clusters. For a discussion of the significance of the results, see Sect. 3.3 of Paper IV.

From the radial surface density distribution $n(r)$ we estimated the richness indicator I_c for each of the 10 fields. This parameter is discussed in more details in Sect. 3.3 of Paper IV and, anyway, it gives an estimate of the total number of cluster members with $K < 15.5$ mag. We list I_c in Table 4, along with other properties of the found clusters and groups of stars: the diameter ($2R$) is obtained from the surface density maps as the geometrical mean of the maximum and minimum extent of the *background* + 1σ level; the peak surface density is derived from the maps of Fig. 13, hence up to the completeness magnitude only, assuming a distance of 700 pc (note that the background surface density accounts for ~240 stars pc^{-2}). Finally, the volume density is estimated by dividing I_c by the volume obtained from the corresponding radius of the density enhancement in Fig. 14. According to such a definition, a close double star would yield a volume density $\sim 5.6 \times 10^4$ stars pc^{-3}; much richer clusters exhibit a lower volume density because of the greater radii.

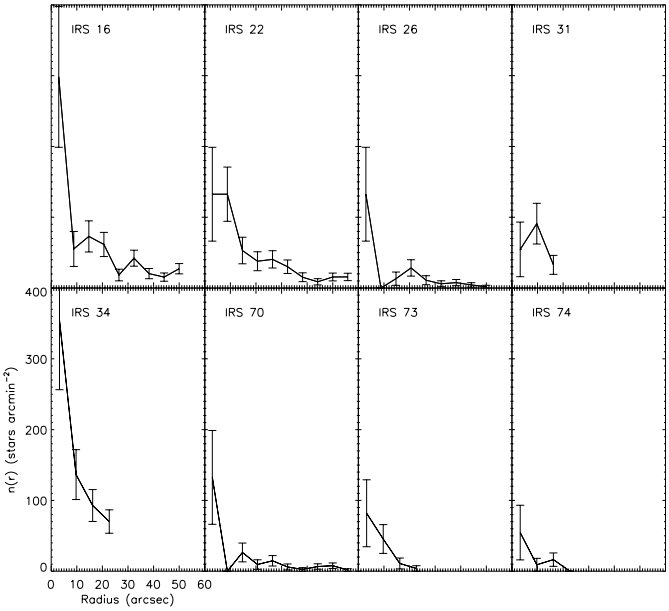

Fig. 14. Radial star surface density $n(r)$, in arcmin^{-2}, versus the projected distance r from the NIR counterpart (arcsec) for 8 fields; $r = 0$ always coincides with the NIR counterparts of the IRAS sources which have been tentatively identified, except for IRS 34 where it has been chosen so at the location of source # 68. The shown error bars indicate the statistical uncertainties.

4. Discussion

4.1. The nature of the IRAS sources

Without counting IRS 16 and IRS 34, in Paper III and herein we carefully analyse a total of 20 IRAS sources fulfilling the selection criteria proposed in Paper I, using *JHK* images and mm data. Hence, we can now attempt a more detailed discussion on their nature. The initial aim of the project, as reported in Paper I, was to find out a sample of relatively massive protostars associated with the VMR and in the evolutionary stage labelled as Class I. The discriminating spectral feature ($dF_\lambda/d\lambda \geq 0$ between 1–20 μm) was then extended to more luminous objects than those usually classified as Class I sources. In point of fact, the idea behind them stems from the theory of low mass star formation and it is not clear at all how much it can be extended to massive star progenitors. Beyond a formal similarity of spectra, we would expect "massive" Class I sources to be young stars still gathering mass, even though most of their bolometric luminosity may be no longer fed by accretion (but, e.g., by hydrogen burning; see Palla & Stahler 1991). Whether in this stage or not, a prototypical object of the sample may be represented by IRS 33. Owing to its isolation, few ambiguities arise: its rising SED from 1 to 60 μm and its location on the colour-colour diagram (lying below the reddening band of main sequence and close to the position of extremely extincted A0 stars), along with the diffuse emission surrounding its NIR counterpart, appear as distinctive features.

It is necessary to check whether the criteria used in Paper I yield a homogeneous sample of objects. Other kinds of young stars clearly have been included in it: possibly, a few Herbig Ae/Be stars (IRS 14, for which see Paper III; IRS 73 and IRS 74), and the selection of IRS 32 and IRS 66 is doubtful (see Sect. 3.1.5). In the framework of a classic scenario, massive Class I sources might be considered as protostars still climbing their birthline (i.e., in a fully accretion phase), whereas Herbig Ae/Be stars have already left the birthline.

A major sample contamination, however, may arise due to UCHII regions. In fact, the constraints on the IRAS colours imposed in Papers I overlap the criterion of Wood and Churchwell (1989). Hence, the sample listed in Paper I might include a number of UCHII regions. Indeed, 8 out of the 20 IRAS sources (and even IRS 16 and IRS 34) fulfil the criterion. In order to test this possibility, the bolometric luminosity is plotted against $\log(F_{60}/F_{12})$ in Fig. 15 for the 20 IRAS sources. The vertical dashed line marks $\log(F_{60}/F_{12}) = 1.3$, one of the constraints given by Wood and Churchwell (1989). We indicated with filled squares all sources meeting the other condition, too [$\log(F_{25}/F_{12}) \geq 0.57$]. Clearly, most of the objects at the high luminosity end have FIR colours typical of UCHII regions (the most luminous ones are also labelled). Increasing the bolometric luminosity, the selection criteria of Paper I join those for UCHII regions. Even though still associated with very young evolutionary stages, UCHII regions are generally believed to be excited by massive stars *already* on the ZAMS. The horizontal dashed line in Fig. 15 indicates the bolometric luminosity typical of a B2 ZAMS star (Panagia 1973). Note that all points lie below or very close to the line. This suggests that probably

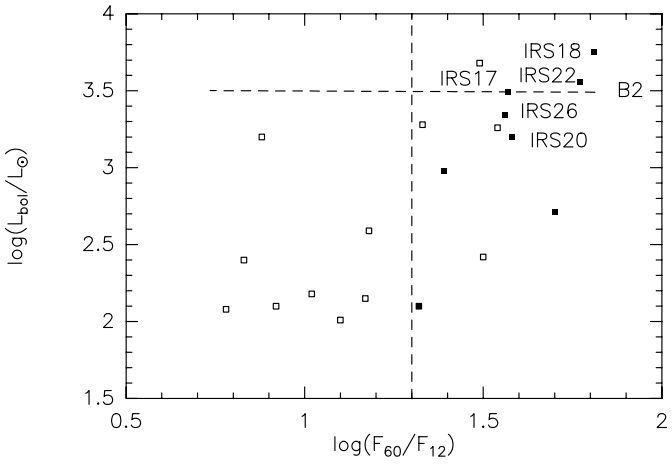

Fig. 15. $L_{\rm bol}$ ($L_\odot$) vs. $\log(F_{60}/F_{12})$ for the 20 Class I source candidates (i.e., IRS 16 and IRS 34 have not been included). Filled squares to the right of the dashed vertical line indicate IRAS sources fulfilling the criterion of Wood & Churchwell (1989) for the selection of UCHII regions. The horizontal dashed line marks the bolometric luminosity of a B2 ZAMS star. The most luminous sources meeting the criterion are also labelled.

none but a few of the most luminous IRAS sources may be stars massive enough to originate a UCHII region. This is confirmed by radio continuum data: none of the 8 IRAS sources meeting the criterion have been detected by the Parkes-MIT survey at 4.85 GHz. This means that their radio flux must lie below 48 mJy (see Griffith & Wright 1994). Using the relation given by Mezger (1978) and assuming $T_{\rm e} = 10000$ K, we may estimate that this upper limit translates into $L'_{\rm c} < 2.09\times10^{45}$ photons s^{-1}, consistent with later than B1 ZAMS stars (Panagia 1973) at a distance of 700 pc. Furthermore, Walsh et al. (1997) searched for methanol masers towards 5 out of the 8 sources with UCHII colours (IRS 13, IRS 17, IRS 18, IRS 20, IRS 22) detecting it from IRS 18 only. They identify this IRAS source as a UCHII region and its ionizing source as a B2 star.

However, the stronger indication that the degree of contamination from UCHII is actually low comes from the fact that towards most of the most luminous IRAS sources with UCHII colours (namely, IRS 13, 17, 20 and 26), the more likely counterparts appear as real stellar objects which are plainly visible in the NIR, whereas UCHII regions are usually not detected at these wavelengths. More generally, IRS 13, 17, 19, 20, 26, 31, 33, 62, 67 and 70 have unambiguous NIR counterparts sharing the same distinctive features (rising SEDs, continuum emission at 1.3 mm, etc.).

In conclusion, the criteria adopted in Paper I allowed to select a sample mostly containing young stellar objects (with an age in the range 10^5–10^6 yr) which appear in the same evolutionary stage. To assess whether they are protostars still accreting their mass is beyond the aim of this paper and needs a more detailed knowledge of their spectra and a suitable modelling. It is also evidenced a moderate sample contamination, mostly by Herbig Ae/Be stars (1–3 sources) and UCHII regions (1?), which however are objects still in a very early evolutionary phase, although slightly older than Class I sources.

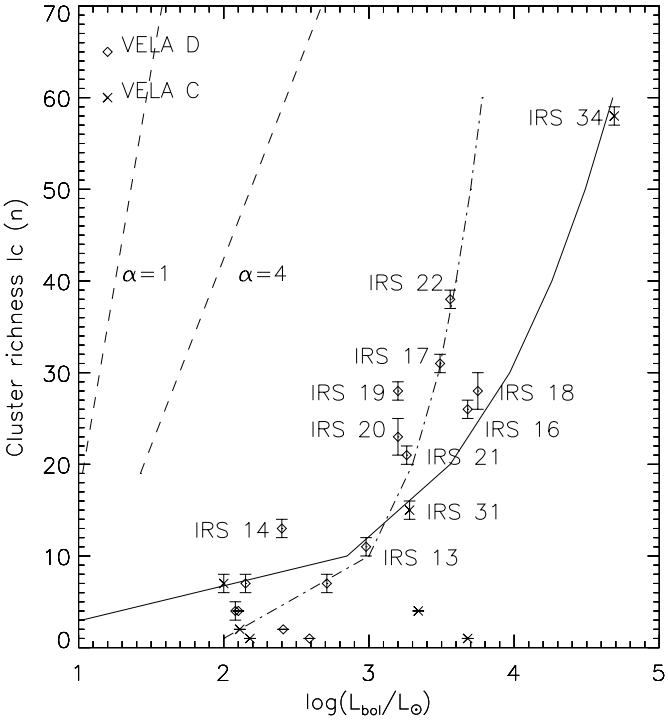

Fig. 16. The richness indicator I_c versus the bolometric luminosity $L_{bol}/L_\odot$; open diamonds are used for the sources associated with cloud D and crosses for those associated with cloud C. Error bars show the propagation of the statistical uncertainty on the sky determination only. The dash-dotted line indicates a $L_{bol} = 10^2 \times I_c\ L_\odot$ relationship, the solid one $L_{bol} = 3.2 \times I_c^{2.35}\ L_\odot$. The dashed lines have been obtained integrating Scalo's IMF times $L/L_\odot = (M/M_\odot)^\alpha$, for $\alpha = 1$ and $\alpha = 4$, as explained in the text.

4.2. The young stellar clusters

The data herein presented for the 10 sites of IRAS sources reinforce our early finding (Paper IV) that young stellar clusters are associated with the most luminous red IRAS sources ($L_{bol} \gtrsim 10^3\ L_\odot$) in the VMR, although even towards some of the less luminous ones small compact groups of young stellar objects are often possibly found. In particular, 4 out of the 10 imaged fields (namely, IRS 16, IRS 22, IRS 31 and IRS 34) have been noted to contain quite prominent star clusters. In Fig. 16, the richness indicator I_c is plotted against the bolometric luminosity of the corresponding IRAS source, including the 12 fields from Paper IV (hence, it is an updated version of its Fig. 8). The IRAS sources associated with cloud D are indicated with open diamonds, those associated with cloud C with crosses. We slightly revised the region of the VMR to which each source belongs (see Table 2 and Fig. 1) on the basis of the latest CO maps available (Yamaguchi et al. 1999). The sources associated with the most prominent clusters are labeled, too, in figure.

Although we do not discuss colour-colour and magnitude-colour diagrams as in Paper IV, it is obvious (see, e.g. Figs. 3a to 12a) that also the newly found clusters show a stellar population which appears to be composed of reddened main sequence stars, Class II and Class I sources. Hence, there coexist objects in different evolutionary stages. In both samples of fields (i.e., the one herein presented and that of Paper III/IV), we often find more than one Class I sources and/or more than one NIR sources that might contribute to the FIR flux. But, based on the steeply rising SEDs in the NIR, complemented, in a few cases, with images at wavelengths longward of K (which we do not present), only one of these objects per field does seem to emerge as the main contributor to the IRAS flux. This is a critical point in interpreting Fig. 16, since it enables us to state that most of L_{bol} is due to a single object (or a small unresolved system of young stellar objects). In this case, given that the luminosities are typical of relatively large (proto-)star masses, our data confirm two well known observational results (see, e.g., Testi et al. 1999): first, that intermediate-mass and massive stars form preferentially within clusters, and next, that the most massive objects are found in the richest clusters.

The point above, that most of the FIR flux arises from a single (or a small group of) young massive object(s), might in principle be tested by investigating the relationship between L_{bol} and the number of cluster members. In Fig. 16, an $L_{bol} \sim I_c$ curve (dot-dashed line) and an $L_{bol} \sim I_c^{2.35}$ one (solid line) are overlaid on the data. The two laws bracket the extreme cases in which, i) all clusters are made of stars of the same mass and age equally contributing to L_{bol} and, ii) all clusters have an IMF like Scalo's (1998) and L_{bol} is equal to that of the most massive star only. Both appear roughly consistent with the data.

The trend shown in Fig. 16 would reflect the L_{bol} vs. N_{tot} relationship if the largest errors were systematic. As for L_{bol}, this means that the uncertainty in the distance of the VMR as a whole is the dominant error, which is reasonable. Also, if the fraction of cluster members retrieved is roughly constant in all frames, we may assume

$$N_{tot} = a \times I_c, \quad (a > 1) \tag{1}$$

which is partly justified by having imaged fields at the same distance with the same sensitivity. The constancy of a is discussed later on.

Let us suppose for the time being that $L_{bol} \sim I_c^b$ is the same as $L_{bol} \sim N_{tot}^b$. The case of all clusters made of stars with the same mass and age and equally contributing to L_{bol} ($b = 1$) is easy to formulate. The other case, in which L_{bol} is entirely provided by the most massive of cluster members ($b = 2.35$) can be obtained according to the following considerations. We can roughly estimate the mass of the most massive star, M_{max}, as a function of N_{tot} by integrating the IMF (normalized in area to the total number of members) from M_{max} to ∞ and imposing the result to be equal to 1. Note that in doing so, we assume M_{max} to be the lowest mass in the integration interval. It is easy to check that, for $dN/dM \sim m^{-\gamma}$ and $L \sim M^\alpha$, we get:

$$L_{bol} \sim N_{tot}^{\frac{\alpha}{\gamma-1}} \tag{2}$$

irrespective of the detailed shape of the IMF in the range $M \leq M_{max}$. For the IMF of Scalo (1998), and assuming $\alpha = 4$, we get $\alpha/(\gamma - 1) = 2.35$ in the range 1–10 $M_\odot$. This result still holds if the bolometric luminosity of the IRAS sources is provided by the group of the most massive stars in the clusters.

It is easily understood how the naive assumption that all the cluster members contribute the same fraction of their bolometric luminosity to the FIR flux measured in the IRAS bands cannot lead to $b = 1$, unless the cluster's IMF is strongly peaked. This can be analytically checked just integrating on the IMF of Scalo (1998) and assuming a $L \sim M^4$ relation for the stars. It is found that the total luminosity of a cluster, $L_{\rm tot}$ increases with the mass of the most massive star (hence, with $N_{\rm tot}$); e.g., we obtained $L_{\rm tot}$ ranging from $\sim 0.5 N_{\rm tot}$ to $\sim 66 N_{\rm tot}$ $L_\odot$ for $M_{\rm max}$ between 2 and 15 $M_\odot$. Clearly, these values are more sensitive to the luminosity-mass relation than to the detailed shape of the IMF. Hence, it appears at least curious that a number of points in Fig. 16 (IRS 17, IRS 19, IRS 20, IRS 21, IRS 22) lie on the $b = 1$ curve, given that the K-band luminosity functions (KLFs) discussed in Paper IV show that the underlying IMFs are similar to that of field stars. The same conclusion can be drawn from the KLFs obtained for the newly-found clusters, which are not presented herein. However, in Fig. 16 we also plot the $L_{\rm tot}$–$N_{\rm tot}$ relation obtained integrating Scalo's IMF times $L/L_\odot = (M/M_\odot)^\alpha$ for $\alpha = 1$ and $\alpha = 4$. $N_{\rm tot}$ has been estimated from a few values of $M_{\rm max}$ as explained above; the integration of the IMF (multiplied by the mass-luminosity relation) was stopped at $M_{\rm max}$, hence we added a term $(M_{\rm max}/M_\odot)^\alpha$ to account for the integral of the IMF from $M_{\rm max}$ to ∞ having explicitly been set to 1. Although $I_{\rm c}$ underestimates $N_{\rm tot}$, the clusters appear overluminous. This is expected if a large fraction of their members are pre-main sequence stars, since these are more luminous than main-sequence stars (whose L–M relation has been used). If offsets are applied to correct for the two effects, the clusters probably fall within the curves defined by $\alpha = 1$ and $\alpha = 4$, showing that their IMF is indeed compatible with Scalo's (1998).

Any conclusion which can be drawn from b in Fig. 16 relies on the assumption that a, the ratio of $N_{\rm tot}$ to $I_{\rm c}$, is roughly constant. $I_{\rm c}$ has been derived by Testi et al. (2001) for 6 of our fields from $K_{\rm s}$ images taken with SOFI at NTT (ESO, La Silla), which are deeper (up to an estimated completeness limit $K \sim 18$ mag) and have a larger field of view ($4' \times 4'$) than ours. As stressed by the authors, it is quite likely that all the cluster members lie below the completeness magnitude, hence an $I_{\rm c}$ determined in this way should approximate very well the true $N_{\rm tot}$. Based on these data, the factor a in Eq. (1) ranges between 1.2 and 4.2, too much to preserve the actual $L_{\rm bol}$-$N_{\rm tot}$ relationship. Nevertheless, we suggest this relationship as a test of the IMF at the highest masses of young embedded star cluster. In fact, if it can be assumed that $L_{\rm bol}$ as obtained from the FIR and sub-mm flux is provided by the most massive stars, then from Eq. (2), $b = \alpha/(\gamma - 1)$. Hence, e.g., if the clusters' IMF was much steeper than Scalo's (1998) at the highest masses, even $b = 1$ would still agree with the observational fact that in each field the IRAS flux is provided by only one or few massive protostars.

Another of the features already remarked in Paper IV is shown in Fig. 13: all identified or proposed IRAS counterparts tend to lie close to the peaks of surface star density. Hence, they are located near the centre of the clusters. If these objects are real precursors of intermediate mass stars, then also their birthplaces must be located close to the centre of the clusters. Note that the most massive stars in the more evolved clusters towards IRS 16 and IRS 34 are located close to the centre, too, suggesting that mass segregation does exist throughout the whole sample of clusters, irrespective of their ages. This has been already evidenced in other young clusters by observations and is predicted by a few models of protostar growth in clusters (see, e.g., Bonnell et al. 1997 and Bonnell & Davies 1998). Possible formation of massive stars far from the cluster in IRS 34 may be interpreted as induced by the expanding HII regions and asks for more in-depth investigation. In the case of IRS 26, the young massive star is located southeast of the surface density peak, where Burkert et al. (2000) find evidence for a strong decrease of extinction from the south-east to the north-west. Hence, the location of the peak may just reflect this morphological feature and IRS26/# 15 could be even closer to the centre of an associated heavily-reddened cluster than is apparent.

The last issue raised in Paper IV concerns the coevality of massive stars in the richer clusters. This is based on the lack of both rich clusters with low $L_{\rm bol}$ ($< 10^3$ $L_\odot$) and isolated IRAS sources with $L_{\rm bol} > 10^3$ $L_\odot$ in the sample of IRAS sources. The data from the present sample seem to confirm that finding. Although we observe stars at the lower end of the intermediate mass range ($L_{\rm bol} < 10^3$ $L_\odot$) forming in isolation (like IRS 33), it appears that intermediate-mass and massive star formation, when in clusters, does not occur *before* the birth of low mass stars. In fact, we have already interpreted the increase of $L_{\rm bol}$ with $N_{\rm tot}$ towards the clusters in terms of the presence of intermediate-mass (proto)stars. Considering that the sample selection based on the IRAS PSC appears to yield a detection limit $L_{\rm bol} \sim 10^2$ $L_\odot$ (roughly consistent with a mass limit $M \sim 3.5$ $M_\odot$), the absence of rich clusters with low $L_{\rm bol}$ may be due to the fact that such clusters cannot be detected until intermediate mass stars begin to grow increasing the FIR flux above the detection limit. This is reinforced by the observational fact that none of the NIR counterparts of the most luminous IRAS sources in our sample are found in isolation. We note that the occurrence of isolated sources at the lower end of the IRAS luminosity range cannot be due to sensitivity issues. In Paper IV, we estimated that the mass of a 10^5 years old pre-main sequence star at our K completeness limit (15.5 mag) is ~ 0.3 $M_\odot$ for an extinction $A_V = 30$ mag. Using the same set of tracks as Paper IV, this mass increases only to ~ 0.5 $M_\odot$ for 10^6 years old pre-main sequence stars, but lower values are obtained, e.g., using the tracks given by Palla & Stahler (1999) or Baraffe et al. (1998; in this case, ~ 0.45 $M_\odot$ for a 2×10^6 years old pms star). As discussed in Sect. 2.2, our K completeness limit is quite a conservative choice and we expect our imaging to be much deeper towards relatively uncrowded areas, so we would not be missing large fractions of young low-mass stars associated with the "isolated" IRAS sources, even if the distance to the VMR was underestimated.

We ruled out the possibility that some of the lower luminosity, isolated, IRAS sources might be intermediate star progenitors preceding the birth of a whole rich cluster on the basis of Fig. 11 in Paper IV. This latter shows the bolometric luminosity vs. the 1.3 mm flux towards the 12 IRAS sources studied in Paper IV. The updated version of the diagram is presented in Fig. 17 where we added 7 out of the 10 targets herein discussed

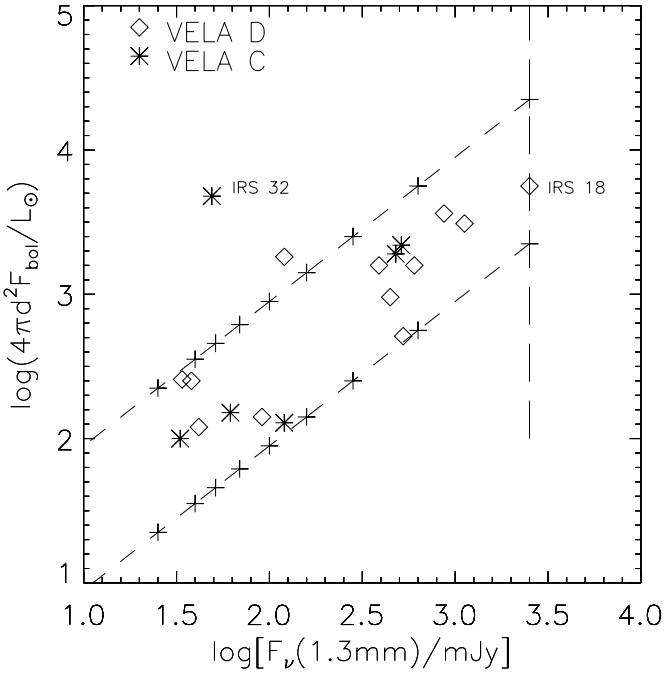

Fig. 17. Bolometric flux vs. 1.3 mm flux for 18 IRAS sources (11 studied in Paper IV and 7 from the present work, all the ones with measurements at 1.3 mm). The bolometric flux is given in solar luminosities assuming a standard distance of 700 pc. The sources associated with cloud C are shown as asterisks, those associated with cloud D as diamonds. The points corresponding to IRS 32 and IRS 18 are labelled. Short-dashed lines indicate the effects of distance on sources with the same bolometric luminosity as IRS 18 (dashed line) and have been chosen such as to roughly enclose all data points (varying the bolometric flux). Crosses on the short-dashed lines mark, from the vertical line, distances 1, 2, 3, 4, 5, 6, 7, 8 and 10 times that of IRS 18.

(all those with measurements at 1.3 mm; IRS 16, IRS 34 and IRS 70 are then excluded). Clearly, if the mm flux not only reflects dust emission from a circumstellar envelope but also catches a consistent degree of emission from the parent molecular cores, then lower luminosity IRAS sources are also associated with less massive cores. If the lower luminosity objects were the earliest members of rich clusters still to be formed, we would expect the opposite trend, i.e., higher mm flux at lower $L_{\rm bol}$. Actually, the increase of mm flux with $L_{\rm bol}$ could be caused by an enhancement of dust temperature because of the presence of massive young stars, rather than a larger gas and dust mass. However, it is easy to check (e.g., from Eq. (1) of Paper III) that dust temperature as a whole should roughly increase from 30 K to at least 200 K in order that the gas mass towards higher and lower luminosity IRAS sources may coincide. Even so, consider that where clusters are already formed a much larger fraction of the parental gas mass has been dissipated due to the star formation processes. In Fig. 17 we also investigate the effect of distance on the result. The skew dashed lines show where a source like IRS 18 would appear in the diagram if located at greater distances but erroneously believed as far as IRS 18 itself. The crosses mark actual distances 2, 3, 4, 5, 6, 7, 8 and 10 times that of IRS 18. If the lower luminosity IRAS sources were objects as luminous as IRS 18 whose distance is just underestimated, it appears that the underestimate should be extremely large (at least of a factor 5, as it can be seen for the group of points with $L_{\rm bol} \sim 10^2\ L_\odot$ in Fig. 17), which is quite unlikely.

Hence, we can conclude that star formation in clusters either is roughly coeval (or accelerated, as proposed by Palla & Stahler 2000), or massive stars form or leave the birthline later than low mass stars, although some of the less massive among the intermediate-mass star progenitors are also observed in isolation.

5. Conclusions

We have presented new *JHK* images and photometry, along with pointed observations at 1.3 mm, of 10 fields towards red IRAS sources mostly associated with cloud C in the VMR. The sample is composed of 7 objects classified as Class I sources in Papers I and II, 2 FIR sources associated with HII regions and a previously unrecognized Class I source. We studied the location of the imaged NIR objects with respect to the IRAS uncertainty ellipses, their NIR colours and their SEDs in order to identify the counterparts of the IRAS sources following the criteria already used in Paper III. We find that:

1. a NIR counterpart can be identified towards 5 IRAS sources (IRS 22, IRS 26, IRS 31, IRS 33 and IRS 70);
2. the main ionizing sources of the 2 HII regions are NIR sources whose colours and magnitudes are consistent with a B0-B5 star (IRS 16) and an O5-B0 star (IRS 34), on the ZAMS or the main sequence. The FIR flux may arise either from UCHII regions or from circumstellar dust heated by the UV radiation, although a Class I source very close to the main ionizing star cannot be excluded in the case of IRS 16;
3. IRS 70 appears as a Class I source associated with cloud D and therefore should be included in the catalogue of Paper I and II;
4. no NIR counterparts can be identified towards IRS 73 and IRS 74. In both cases possible Herbig Ae/Be stars are imaged and the FIR emission could be due to circumstellar dust associated with them;
5. the nature of IRS 32 is difficult to assess. No NIR candidates could be identified; the flux at 100 μm is an upper limit and, hence, its $L_{\rm bol}$ is an overestimate. It lies at the border of an HII region.

The nature of the 12 IRAS sources examined in Paper III and 8 of the ones herein presented (including IRS 70), all meeting the criteria defined in Paper I, has been reviewed and discussed. Although 8 out of 20 IRAS sources fulfil the criterion of Wood & Churchwell (1989), the contamination from UCHII regions is believed to be low. A small contamination due to Herbig Ae/Be stars has also been found (IRS 14 and, possibly, IRS 73 and IRS 74). But most of the sources in the sample are probably genuine precursors of intermediate mass stars ($\sim 2-10\ M_\odot$) which may still be in an accretion stage (i.e., Class I sources). From the difference between the NIR colours of associated reflection nebulae and theirs, we found that some of them must

Table 5. *JHK* photometry and positions of found *K* sources towards IRS 32, given as an example of the whole list in electronic form at the CDS.

NIR source	RA(2000) (^{h} ^{m} ^{s})	δ(2000) ($^\circ$ $'$ $''$)	*J*	*H* (mag)	*K*
1	8 59 18.63	−43 42 48.6	12.75 ± 0.00	11.71 ± 0.00	11.15 ± 0.00
2	8 59 23.81	−43 42 47.1	> 19.50	18.08 ± 0.17	16.76 ± 0.10
3	8 59 20.24	−43 42 46.6	> 19.50	17.55 ± 0.08	16.43 ± 0.08
4	8 59 20.79	−43 42 45.8	14.46 ± 0.00	12.85 ± 0.00	11.85 ± 0.00
5	8 59 21.71	−43 42 43.5	> 19.50	> 18.80	17.09 ± 0.15
6	8 59 20.00	−43 42 38.5	> 19.50	17.75 ± 0.12	16.39 ± 0.07
7	8 59 23.46	−43 42 34.9	16.38 ± 0.03	14.20 ± 0.00	12.75 ± 0.00
8	8 59 21.30	−43 42 31.6	18.88 ± 0.21	15.72 ± 0.02	14.30 ± 0.01
9	8 59 19.54	−43 42 30.8	> 19.50	18.04 ± 0.16	16.41 ± 0.07
10	8 59 21.98	−43 42 30.5	15.51 ± 0.01	13.99 ± 0.00	13.26 ± 0.00
11	8 59 18.99	−43 42 28.9	16.24 ± 0.02	15.08 ± 0.01	14.40 ± 0.01
12	8 59 21.12	−43 42 24.8	19.39 ± 0.35	16.77 ± 0.05	15.56 ± 0.04
13	8 59 21.73	−43 42 23.9	17.23 ± 0.05	15.98 ± 0.03	15.07 ± 0.02
14	8 59 19.18	−43 42 11.0	17.95 ± 0.10	14.55 ± 0.01	12.71 ± 0.00
15	8 59 22.86	−43 42 6.0	> 19.50	18.64 ± 0.30	17.32 ± 0.21
16	8 59 19.36	−43 42 2.9	19.56 ± 0.44	16.61 ± 0.04	14.74 ± 0.02
17	8 59 20.52	−43 41 60.0	0.00 ± 0.00	17.20 ± 0.07	15.60 ± 0.04
18	8 59 22.08	−43 41 57.7	16.80 ± 0.03	15.01 ± 0.01	14.09 ± 0.01
19	8 59 22.92	−43 41 57.5	> 19.50	16.88 ± 0.06	15.42 ± 0.03
20	8 59 18.84	−43 41 50.6	> 19.50	17.50 ± 0.13	16.18 ± 0.07
21	8 59 19.99	−43 41 43.6	> 19.50	16.97 ± 0.07	15.77 ± 0.06
22	8 59 23.72	−43 42 37.5	> 19.50	> 18.80	17.79 ± 0.33
23	8 59 23.26	−43 42 19.0	> 19.50	> 18.80	16.96 ± 0.16
24	8 59 23.63	−43 42 18.2	> 19.50	> 18.80	18.19 ± 0.44

be heavily reddened. Along with the morphology of the diffuse emission, this suggests that large (edge-on) circumstellar disks may accompany the protostars in at least 2 cases (namely IRS 20 and IRS 26).

At last, we found young stellar clusters towards the most luminous of the IRAS sources. The richest ones are in the fields of IRS 16, IRS 22, IRS 31 and IRS 34. This confirms the results of Paper IV, i.e. that young stellar clusters are associated with the IRAS sources selected in Paper I and II which have $L_{\rm bol} \gtrsim 10^3\ L_\odot$. The properties of the clusters are similar to those derived in Paper IV: the sizes are $\gtrsim 0.1$ pc, the peaks of star surface density are $\sim 10^3$ stars pc^{-2} and the star volume density is in the range 10^3–10^4 stars pc^{-3}. Also the lower luminosity IRAS sources often seem to be associated with small compact groups of NIR objects, but what appears as a lonesome Class I source (IRS 33) with $L_{\rm bol} \sim 150\ L_\odot$ suggests that stars with $M \sim 3.5\ M_\odot$ can still form in relative isolation. Some preliminary findings of Paper IV have been herein confirmed:

1. more massive (proto)stars are embedded in richer clusters;
2. when not isolated, intermediate mass (proto)stars tend to be located near the cluster centre;
3. the most massive stars in a cluster do not appear to form before the low mass ones.

A relation $L_{\rm bol} \sim N_{\rm tot}^b$ is suggested by our data between the bolometric luminosity of the associated IRAS source and the total number of cluster members. In the case of clusters with a Scalo (1998) IMF where the FIR flux was contributed by the most massive stars, we would expect $L_{\rm bol} \sim N_{\rm tot}^{2.35}$, but due to the difficulty found in deriving $N_{\rm tot}$ from $I_{\rm c}$, it has not been possible to estimate b from our data.

Acknowledgements. We thank Prof. Y. Fukui and the other authors of the paper for kindly allowing us to reproduce Fig. 1b from Yamaguchi et al. (1999).

References

Allen, C. W. 1976, Astrophysical Quantities, 3rd edn. (Athlone press, London)
Baraffe, I., Chabrier, G., Allard, F., & Hauschildt, P. H. 1998, A&A, 337, 403
Bonnell, I. A., Bate, M. R., Clarke, C. J., & Pringle, J. E. 1997, MNRAS, 285, 201
Bonnell, I. A., & Davies, M. B. 1998, MNRAS, 295, 691
Braz, M. A., & Epchtein, N. 1982, A&A, 111, 91
Braz, M. A., & Scalise, E. Jr. 1982, A&A, 107, 272
Bronfman, L., Nyman, L.-A., & May, J. 1996, A&AS, 115, 81
Burkert, A., Stecklum, B., Henning, Th., & Fischer, O. 2000, A&A, 353, 153
Caswell, J. L., & Haynes, R. F. 1987, A&A, 171, 261
Griffith, M. R., & Wright, A. E. 1993, AJ, 105, 1666
Haynes, R. F., Caswell, J. L., & Simons, L. W. J. 1979, AuJPAS, 48, 1
Koornneef, J. 1983, A&A, 128, 84
Kreysa, E. 1990, Sub-mm Direct Photometry with Large Telescopes, in From Ground-Based to Space-Born Submm Astronomy. Proc. of the 29th Liege Symp. 3-5 July 1990, ESA SP-314, 265
Lada, C. J., & Wilking, B. A. 1984, ApJ, 287, 610

Liseau, R., Lorenzetti, D., Nisini, B., Spinoglio, L., & Moneti, A. 1992, A&A, 265, 577 (Paper I)
Lorenzetti, D., Spinoglio, L., & Liseau, R. 1993, A&A, 275, 489 (Paper II)
Lorenzetti, D., Giannini, T., Vitali, F., Massi, F., & Nisini, B. 2002, ApJ, 564, 839
Massi, F., Giannini, T., Lorenzetti, D., et al. 1999, A&AS, 136, 471 (Paper III)
Massi, F., Lorenzetti, D., Giannini, T., & Vitali, F. 2000, A&A, 353, 598 (Paper IV)
Mezger, P. G. 1978, A&A, 70, 565
Moorwood, A., Finger, G., Biereichel, P., et al. 1992, ESO Mess., 69, 61
Moriguchi, Y., Yamaguchi, N., Onishi, T., Mizuno, A., & Fukui, Y. 2001, PASJ, 53, 1025
Murphy, D. C., & May, J. 1991, A&A, 247, 202
Palla, F., & Stahler, S. W. 1991, ApJ, 375, 288
Palla, F., & Stahler, S. W. 1993, ApJ, 418, 414
Palla, F., & Stahler, S. W. 1999, ApJ, 525, 772
Palla, F., & Stahler, S. W. 2000, ApJ, 540, 255
Panagia, N. 1973, AJ, 78, 929
Rieke, G. H., & Lebofsky, M. J. 1985, ApJ, 288, 618
Scalo, J. 1998, The IMF Revisited: A Case for Variations, in The Stellar Initial Mass Function, Proc. of the 38th Herstmonceux Conf., ed. G. Gilmore, & D. Howell, ASP Conf. Ser., 142, 201
Testi, L., Palla, F., & Natta, A. 1999, A&A, 342, 515
Testi, L., Vanzi, L., & Massi, F. 2001, ESO Mess., 103, 28
Verma, R. P., Bisht, R. S., Ghosh, S. K., et al. 1994, A&A, 284, 936
Walsh, A. J., Hyland, A. R., Robinson, G., & Burton, M. G. 1997, MNRAS, 291, 261
Weinberger, R., Saurer, W., & Seeberger, R. 1995, A&AS, 110, 269
Wood, D. O. S., & Churchwell, E. 1989, ApJ, 340, 265
Wouterloot, J. G. A., & Brand, J. 1999, A&AS, 140, 177
Yamada, T., Takata, T., Djamaluddin, T., et al. 1993, ApJS, 89, 57
Yamaguchi, N., Mizuno, N., Saito, H., et al. 1999, PASJ, 51, 775
Zinchenko, I., Henkel, C., & Mao, R. Q. 2000, A&A, 361, 1079